© 2022. Published by The Company of Biologists Ltd | Development (2022) 149, dev200597. doi:10.1242/dev.200597

RESEARCH ARTICLE

# Pinch2 regulates myelination in the mouse central nervous system

**Joana Paes de Faria[1,2,*], Raquel S. Vale-Silva[1,2,3], Reinhard Fässler[4], Hauke B. Werner[5] and João B. Relvas[1,2,6,*]**

## ABSTRACT

The extensive morphological changes of oligodendrocytes during axon ensheathment and myelination involve assembly of the Ilk-Parvin-Pinch (IPP) heterotrimeric complex of proteins to relay essential mechanical and biochemical signals between integrins and the actin cytoskeleton. Binding of Pinch1 and Pinch2 isoforms to Ilk is mutually exclusive and allows the formation of distinct IPP complexes with specific signaling properties. Using tissue-specific conditional gene ablation in mice, we reveal an essential role for Pinch2 during central nervous system myelination. Unlike *Pinch1* gene ablation, loss of Pinch2 in oligodendrocytes results in hypermyelination and in the formation of pathological myelin outfoldings in white matter regions. These structural changes concur with inhibition of Rho GTPase RhoA and Cdc42 activities and phenocopy aspects of myelin pathology observed in corresponding mouse mutants. We propose a dual role for Pinch2 in preventing an excess of myelin wraps through RhoA-dependent control of membrane growth and in fostering myelin stability via Cdc42-dependent organization of cytoskeletal septins. Together, these findings indicate that IPP complexes containing Pinch2 act as a crucial cell-autonomous molecular hub ensuring synchronous control of key signaling networks during developmental myelination.

**KEY WORDS: Integrin signaling, IPP complex, Myelin, Small Rho GTPases, Oligodendrocyte, Central nervous system**

## INTRODUCTION

In the central nervous system (CNS), oligodendrocytes (OLs) form myelin, a specialized cytoplasmic membrane growing around axons that ensures fast and effective propagation of action potentials along axons (Nave and Werner, 2014; Snaidero and Simons, 2017). The molecular signals regulating myelination derive, at least in part, from instructive cues originating from the extracellular matrix (ECM) and transduced by integrin transmembrane receptors. This signaling is initiated by ligand occupation and clustering of integrin subunits in topographically discrete regions of the membrane, and mediated through molecular scaffolds, such as the heteroternary Ilk-Parvin-Pinch (IPP) complex in focal adhesions (Legate et al., 2006; Wickström et al., 2010; Qin and Wu, 2012; Wu, 2004). In association with other molecules, such as paxillin, talin, vinculin and tensin, this protein complex links the ECM with the actin cytoskeleton by regulating the activity of downstream molecules, including Rho GTPases, profilin 1, Jab1 (Cops5) or N-Wasp (Wasl) (Feltri et al., 2016). The IPP complex contains integrin linked kinase (Ilk), the adaptor protein five LIM (LIN-11, Isl-1, MEC-3) domain-containing Pinch ('particularly interesting Cys-His-rich protein') proteins and the F-actin-binding proteins parvins. The interaction between Pinch and Ilk proteins, which occurs prior to the formation of cell-ECM adhesion complexes in the cell membrane independently of adhesion signals (Zhang et al., 2002b), is necessary to prevent proteasome-mediated degradation of the IPP complex (Fukuda et al., 2003). In mammalian cells, IPP function depends on the mutually exclusive binding (Li et al., 1999; Zhang et al., 2002a) of Pinch1 (Lims1) (Rearden, 1994; Tu et al., 1999) or Pinch2 (Lims2) (Hobert et al., 1999; Zhang et al., 2002a), and forms a signaling hub controlling essential cell functions such as cell-ECM contact and adhesion, organization of the cytoskeleton, survival, proliferation and migration in various cellular contexts (Legate et al., 2006). Encoded by distinct genes, the two proteins have high sequence similarity (Braun et al., 2003), and are co-expressed in various tissues (Rearden, 1994; Braun et al., 2003). Pinch1 is highly and mostly exclusively expressed in early embryonic stages, whereas Pinch2 is detected from the midgestational stage (Braun et al., 2003). The two Pinch isoforms have different binding partners (Kadrmas et al., 2004; Dougherty et al., 2005; Vaynberg et al., 2005; Velyvis et al., 2003; Wiesner et al., 2005; Guo et al., 2019), recruitment of which likely confers signaling specificity to the IPP complex.

In the peripheral nervous system, Ilk is required for the developmental radial sorting of axons out of bundles through negative regulation of Rho/Rho kinase signaling (Pereira et al., 2009). In OLs, Ilk is required for laminin-2-induced formation of myelin-like membrane formation (Chun et al., 2003) and regulates process extension by regulating OL actin cytoskeletal dynamics (O'Meara et al., 2013; Michalski et al., 2016). *In vivo*, Ilk ablation disturbs OL precursor cell (OPC) proliferation and differentiation (Hussain and Macklin, 2017). However, as it prevents assembly of the IPP complex it also leads to the degradation of the other IPP components, making it impossible to dissect the exact role played by Pinch1 and Pinch2 in OL development. Here, we ablated either *Pinch1* or *Pinch2* in the mouse OL lineage to investigate their specific functions during myelination. Our results support an essential function of Pinch2 protein in controlling the development and structure of myelin sheath.

## RESULTS

### Pinch1 and Pinch2 expression is developmentally regulated in OLs

We examined the expression of the two Pinch proteins in the mouse optic nerve (ON), an OL-enriched tissue that follows a well-

[1]Department of Neurobiology and Neurological Disease, Glial Cell Biology Laboratory, Instituto de Biologia Molecular e Celular (IBMC), Universidade do Porto, 4200-135 Porto, Portugal. [2]Department of Neurobiology and Neurological Disease, Glial Cell Biology Laboratory, Instituto de Investigação e Inovação em Saúde (i3S), Universidade do Porto, 4200-135 Porto, Portugal. [3]Instituto de Ciências Biomédicas Abel Salazar (ICBAS), Universidade do Porto, 4050-313 Porto, Portugal. [4]Department of Molecular Medicine, Max Planck Institute of Biochemistry, 82152 Martinsried, Germany. [5]Department of Neurogenetics, Max Planck Institute of Experimental Medicine, D-37075 Gottingen, Germany. [6]Department of Biomedicine, Faculty of Medicine, Universidade do Porto, 4200-319 Porto, Portugal.

*Authors for correspondence (joana.paesdefaria@ibmc.up.pt; jrelvas@ibmc.up.pt)

J.P.d.F., 0000-0001-7046-6197; R.S.V.-S., 0000-0002-4240-376X; R.F., 0000-0002-0145-6937; H.B.W., 0000-0002-7710-5738; J.B.R., 0000-0001-7636-0924

**Handling Editor: François Guillemot**
**Received 29 January 2022; Accepted 16 May 2022**

Development (2022) 149, dev200597. doi:10.1242/dev.200597

established spatiotemporal sequence of events during development (Dangata and Kaufman, 1997; Foran and Peterson, 1992) and in which axons are uniformly aligned. In mice, OPCs migrate from the floor of the third ventricle throughout the developing nerve until around the day of birth; at postnatal day (P) 5 most OPCs are differentiating and myelination of axons initiates around P7. Whereas Pinch1 expression is already detected at P5 (Fig. 1A,B), Pinch2 expression is not detected until later at P15 (Fig. 1A,C). These protein profiles reflect the abundance of their respective RNA molecules in the developing myelinating glia (Zhang et al., 2014). To understand Pinch1 and Pinch2 function in OLs, we generated conditional *Pinch1* and *Pinch2* single conditional knockout (cKO) mice by *in vivo Cre*-mediated recombination. Mouse lines carrying *Pinch1* or *Pinch2* with relevant floxed allelic regions (Li et al., 2005; Stanchi et al., 2005) (Fig. S1A) were crossed with a *Cnp*-driven *Cre* mouse line ($Cnp^{Cre/+}$), where *Cre* is expressed in differentiating myelinating glia from embryonic day 13 (Lappe-Siefke et al., 2003). The resulting cKO progenies $Cnp^{Cre/+}$ $Pinch1^{flox/flox}$ (hereafter referred to as *Pinch1* cKO or *P1* cKO) or $Cnp^{Cre/+}$ $Pinch2^{flox/flox}$ (hereafter referred to as *Pinch2* cKO or *P2* cKO) and the respective littermates, $Pinch1^{flox/flox}$ and $Pinch2^{flox/flox}$ (controls, CTR) were born at the expected Mendelian frequency and displayed no obvious developmental or motor deficits. Conditional recombination of either floxed *Pinch1* or *Pinch2* alleles resulted in significantly decreased protein levels in lysates obtained from P15 ONs (Fig. 1D). The residual levels of Pinch protein detected in the blot are likely due to the presence of astrocytes and low numbers of unrecombined OLs in the tissue (Zhang et al., 2014). The IPP protein complex arises from the association of different proteins, including the exclusive binding of either Pinch1 or Pinch2 to Ilk (Li et al., 1999; Zhang et al., 2002a). Thus, the loss of one Pinch protein does not preclude the assembly of an alternative complex with the existing Pinch, Ilk and Parvin proteins (Fukuda et al., 2003). By immunoblot, we confirmed that in P15 ON the expression levels of Ilk and α-Parvin in *Pinch1* and *Pinch2* cKOs were not significantly different from controls (Fig. 1E,F). This establishes that in the presence of either Pinch, the IPP complex of proteins is formed. Targeting one Pinch gene and depleting its expression did not result in a compensatory increase in the expression of the untargeted Pinch counterpart (Fig. 1G-J), with the conspicuous exception of P15 *Pinch1* cKO ONs, in which Pinch2 expression was transiently increased (0.49±0.18 versus 1.09±0.13, $P$=0.049; Fig. 1G,H), which may be a result of transient accumulation of unbound Ilk molecules and an increase in Pinch2 stability (Stanchi et al., 2005). Altogether, these results show that in OLs, the IPP complex is formed by either Pinch1 or Pinch2 proteins at distinct

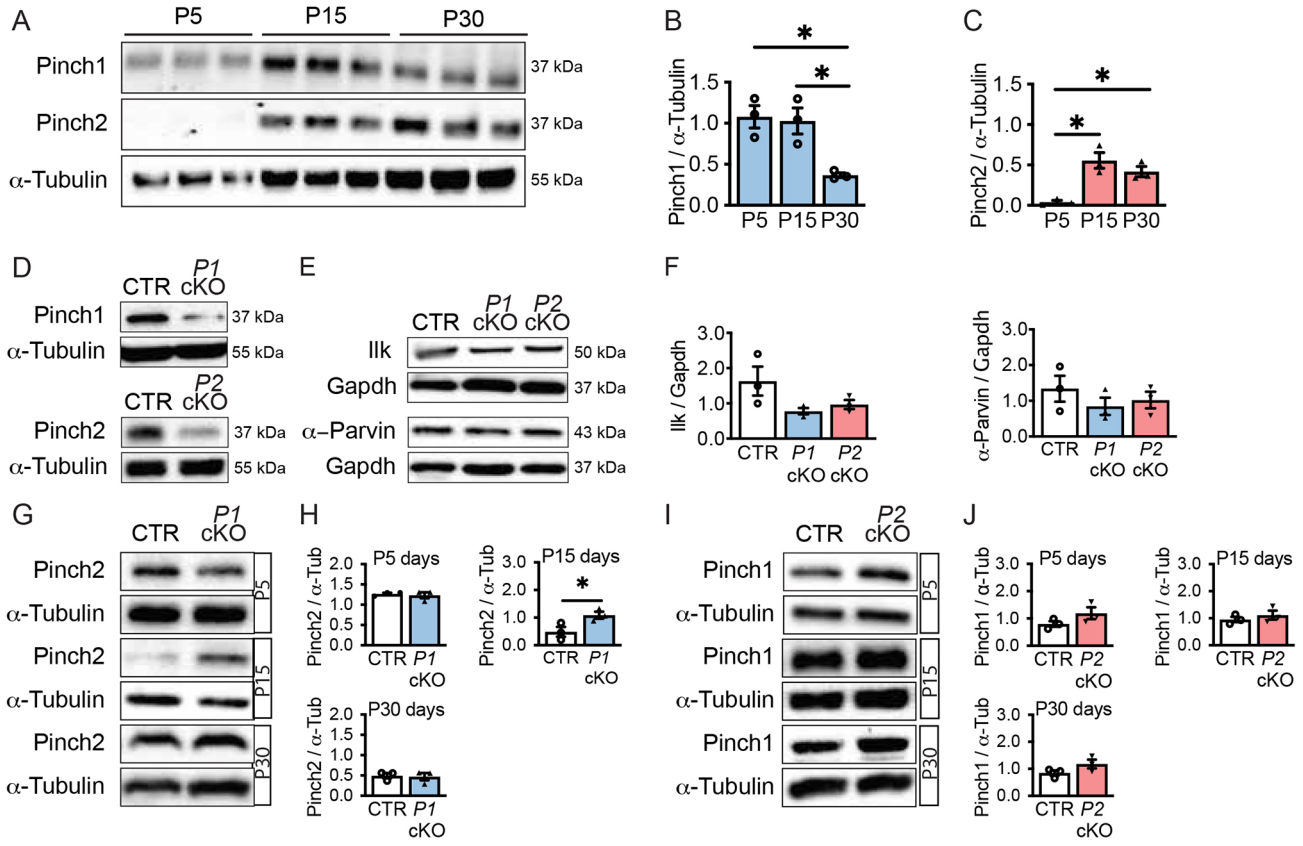


**Fig. 1. Differential expression of Pinch proteins in the developing ON.** (A) Western blot analysis of ON homogenates derived from P5, P15 and P30 wild-type mice (C57BL/6). (B,C) Densitometric analysis of Pinch1 and Pinch2 immunoreactive signals normalized to α-tubulin. Statistical differences were detected between P5 and P30 ($P$=0.019) and between P15 and P30 ($P$=0.019) for Pinch1 and between P5 and P15 ($P$=0.005) and between P5 and P30 ($P$=0.024) for Pinch2. *$P$≤0.05 [one-way ANOVA: $F(2,6)$=10.52, $P$=0.01 and $F(2, 6)$=15.21 $P$=0.004, followed by a Holm–Sidak post-hoc test]; $n$=3. (D) Western blot analysis of Pinch1 and Pinch2 in *Pinch1* cKO ($Cnp^{Cre/+}$:$Pinch1^{flox/flox}$; *P1* cKO) and *Pinch2* cKO ($Cnp^{Cre/+}$:$Pinch2^{flox/flox}$; *P2* cKO) mice, respectively, and the corresponding controls ($Pinch1^{flox/flox}$ and $Pinch2^{flox/flox}$; CTR) at P15. (E,F) No significant changes were detected in the levels of Ilk and α-Parvin in Pinch cKOs compared with CTR. One-way ANOVA $F(2, 6)$=3.11 ($P$=0.11) for Ilk and $F(2, 6)$=0.76 ($P$=0.5) for α-Parvin ($n$=3). (G-J) Immunoblot analysis of ONs from Pinch cKO and CTR mice at P5, P15 and P30 show unchanged levels of the untargeted Pinch, except a transient upregulation of Pinch2 in *P1* cKO ($P$=0.049) (ON, P15). (H,J) *$P$≤0.05 (unpaired, two-tailed Student's $t$-test); $n$=3. (B,C,F,H,J). Error bars represent s.e.m.

Development (2022) 149, dev200597. doi:10.1242/dev.200597

developmental stages, possibly to exert different context-specific functions.

### Axon contact and ensheathment are not affected by the loss of either Pinch1 or Pinch2

To gain insight into the individual contribution of Pinch1 and 2 in developmental myelination, we first examined the myelin ultrastructure of white matter tracts in the ON, brain [midsagittal sections of the corpus callosum (CC)] and spinal cord (SC) at P15, a relatively early stage of developmental myelination, by transmission electron microscopy (TEM).

At P15, despite the loss of either *Pinch1* or *Pinch2*, OLs were able to myelinate axons efficiently in these different anatomical regions (Fig. 2A). In line with this, no significant differences were found in the numbers of contacted axons ($P$=0.77, $n$=5 in *P1* cKO; $P$=0.42, $n$=3/4 in *P2* cKO; Fig. 2B), in the relationships between axon diameter and myelin sheath thickness ($g$-ratio) (0.842±0.001 versus 0.846±0.003, $P$=0.21, $n$=3 in *P1* cKO; 0.849±0.005 versus 0.854±0.005, $P$=0.27, $n$=3 in *P2* cKO; Fig. 2C), or in the diameters of axons (1.04±0.04 versus 1.02±0.03, $P$=0.6, $n$=3 in *P1* cKO; 1.06±0.03 versus 1.04±0.03, $P$=0.8, $n$=3 in *P2* cKO; Fig. S2A) in the ON of Pinch cKOs and their control littermates. These observations suggest that the formation of an IPP complex by either Pinch is sufficient to support the onset and early stages of myelination in the ON.

Ilk (Pereira et al., 2009) and Pinch1 (Eke et al., 2010; Fukuda et al., 2003) were previously described to be required for the activation of Akt, which is also an essential modulator of OPC survival *in vitro* (Flores et al., 2000). However, we did not detect significant changes in the levels of Akt phosphorylation in lysates obtained from ON of P15 *Pinch1* cKO compared with those from controls ($P$=0.26, $n$=3; Fig. S2B). Similarly, the activity of p38 mitogen-activated protein kinase (MAPK), which is also regulated by IPP (Smeeton et al., 2010), remained unchanged in ON lysates from either Pinch cKO ($P$=0.60, $n$=3 in *P1* cKO; $P$=0.68, $n$=4 in *P2* cKO; Fig. S2C). In contrast, the activity of the MAP kinases Erk1/2 (Mapk3/Mapk1) and Jnk (Mapk8) were specifically and transiently upregulated in P15 *Pinch1* cKO (p-Erk: 0.82±0.08 versus 1.14±0.03, $P$=0.018, $n$=3; p-Jnk: 0.24±0.02 versus 0.42±0.05, $P$=0.039, $n$=3; Fig. S2D,E). Because sustained activation of Erk1/2 increases the numbers of OPCs (Ishii et al., 2013), we next examined OPC/OL cells in P15 ONs of both *Pinch1* and *Pinch2* cKOs using the bona fide lineage marker Olig2. We observed a transient increase in Olig2-positive cells in the ON of *Pinch1* cKO (49.8±2.4 versus 59.8±2.2, $P$=0.036, $n$=3; Fig. S2F), but not in *Pinch2* cKO ($P$=0.64, $n$=3; Fig. S2G), which is consistent with the increase in Erk1/2 activity in *Pinch1* cKO. OL lineage expansion co-existed with stable numbers of CC1 (APC)-positive mature oligodendroglia in *Pinch1* cKO (34.2±2.4 versus 40.3±0.7, $P$=0.07, $n$=3; Fig. S2F), suggesting that OPC/OL population growth is paralleled by steady OL differentiation and increased cell death. This was confirmed by the presence of significantly higher numbers of Olig2-positive cells that were also terminal deoxynucleotidyl transferase dUTP nick end labeling (TUNEL)-positive in the ON of *Pinch1* cKO (4.9±0.6 versus 8.9±0.5, $P$=0.0089, $n$=3; Fig. S3A), compared with controls at P30. As Pinch1 inhibits Jnk-mediated apoptosis in mouse primitive endoderm cells (Montanez et al., 2012), and its activation is increased in lysates obtained from *Pinch1* cKO ONs, it is conceivable that a Pinch1-dependent mechanism regulates the OPC/OL pool via Jnk-mediated cell apoptosis. Concomitant with the transient variation in the numbers of Olig2-positive cells, both Erk1/2 and Jnk activities in *Pinch1* cKO returned to control levels by P30 (p-Erk: 1.2±0.1 versus 1.1±0.2, $P$=0.8, $n$=4; p-Jnk: 1.6±0.1 versus 1.4±0.1, $P$=0.3, $n$=3; Fig. S3B,C).

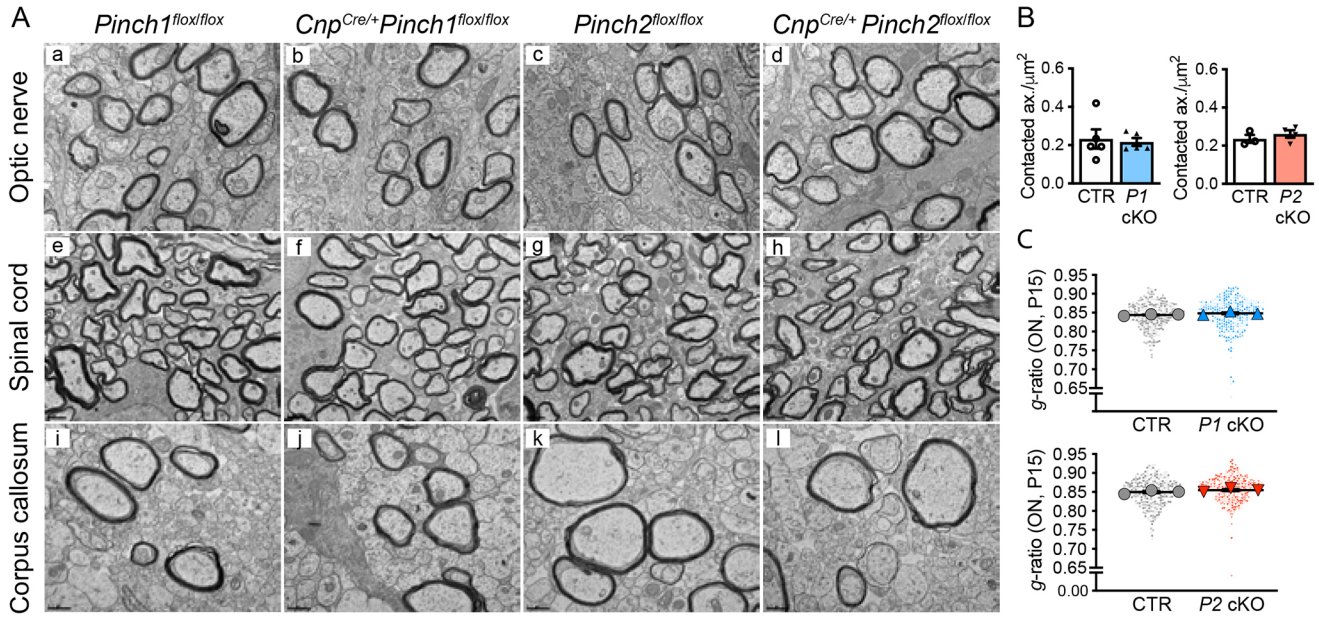


**Fig. 2. Pinch depletion does not prevent axon contact and ensheathment.** (A) Representative electron micrographs of cross-sections of the ON (a-d), SC (e-h) and CC (i-l) from *Pinch1* (*Cnp*$^{Cre/+}$ *Pinch1*$^{flox/flox}$; *P1* cKO; b,f,j) and *Pinch2* (*Cnp*$^{Cre/+}$ *Pinch2*$^{flox/flox}$; *P2* cKO; d,h,l) cKO mice, and from the respective controls (CTR in a,e,i, and c,g,k) at P15. Scale bars: 0.5 µm (ON and CC); 1 µm (SC). (B) A similar number of contacted and/or myelinated axons were observed in the ON from *Pinch1* and *Pinch2* cKOs and CTR mice at P15. Error bars represent s.e.m. (C) No differences in $g$-ratio were detected in cKOs compared with the respective CTRs (measured in ONs at P15). Beeswarm superplots show mean per animal used to calculate the overall average, s.e.m. and $P$-values. (B,C) Statistical analysis used unpaired, two-tailed Student's $t$-test; $n$=3/4 (in C, each $n$ represents at least 300 myelinated axons analyzed per genotype).

Development (2022) 149, dev200597. doi:10.1242/dev.200597

These findings suggest that in the early developing ON, Pinch1 – but not Pinch2 – is involved in the control of OPC/OL population homeostasis, through MAPK-dependent signaling. Because independent ablation of *Pinch1* and *Pinch2* had no obvious impact on axon contact or ensheathment, our results suggest that Pinch proteins are competent in establishing the IPP complex during the onset and early stages of myelination.

### Loss of *Pinch2* results in myelin overgrowth and formation of redundant myelin

We next examined the myelin ultrastructure in cross-sections from ON, SC and CC in young adult mice (P30), a period of active myelination. We observed that in these distinct anatomical regions, the myelin sheaths of *Pinch2* cKO axons were thicker compared with those of control or *Pinch1* cKO axons (Fig. 3A). This was reflected by the significantly lower *g*-ratios found in *Pinch2* cKO (0.811±0.012 versus 0.773±0.0051, $P$=0.015, $n$=3/5; Fig. 3B, Fig. S4A), whereas in *Pinch1* cKO *g*-ratios remained close to control values (0.802±0.008 versus 0.806±0.003, $P$=0.62, $n$=3). Axon calibers did not differ from the respective controls in both cases (Fig. 3C, *Pinch2* cKO versus CTR: $P$=0.17, $n$=3/5; Fig. S4B, *Pinch1* cKO versus CTR: $P$=0.29, $n$=3). In both cKOs, the number of myelinated axons was similar to controls ($P$=0.9, $n$=3 in *P1* cKO; $P$=0.4; $n$=3/5 in *P2* cKO; Fig. S4C). Morphometric analysis of

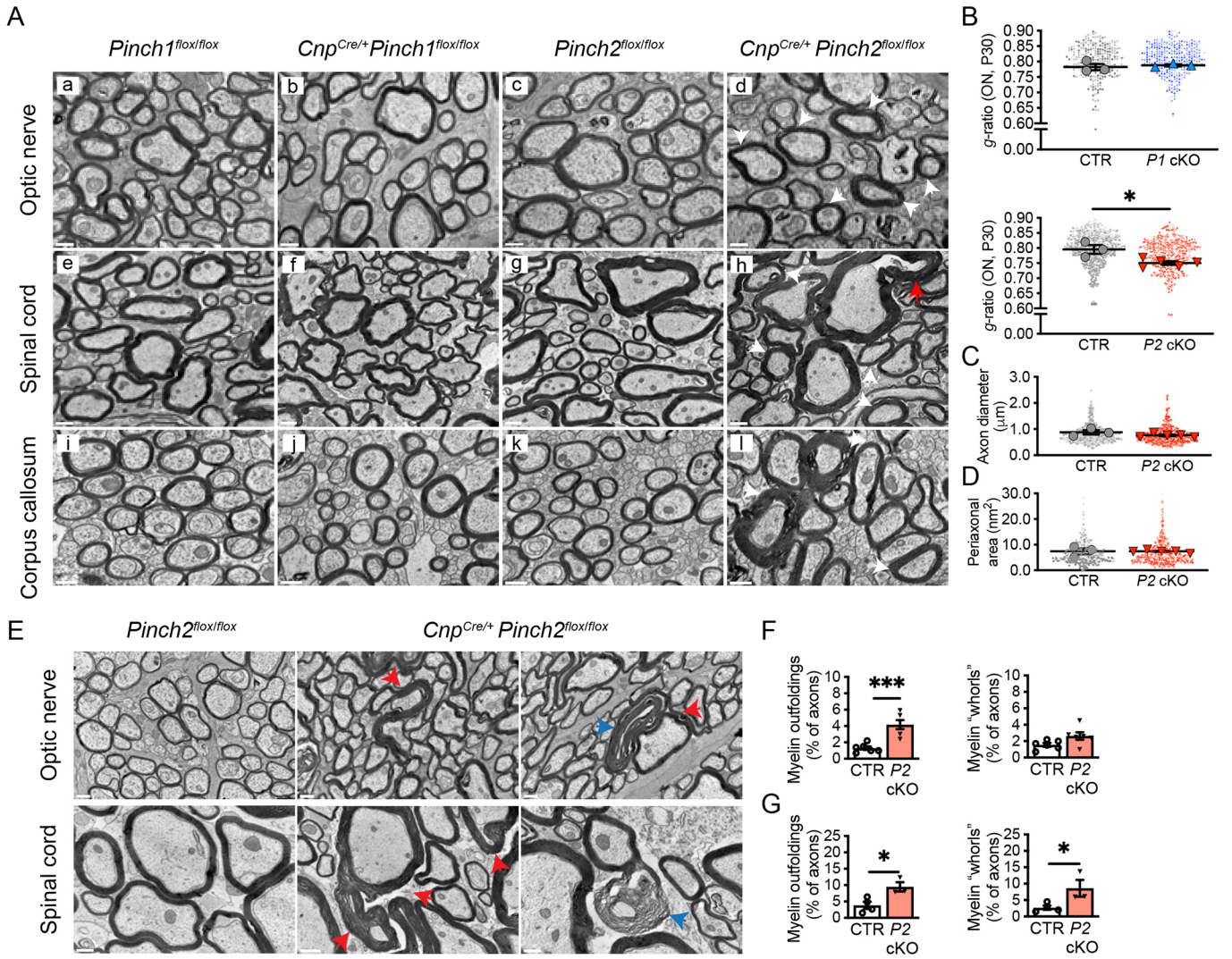


**Fig. 3. OL-specific loss of Pinch2 leads to myelin membrane overgrowth and formation of myelin outfoldings.** (A) Representative electron micrographs of cross-sections of the ON (a-d), SC (e-h) and CC (i-l) from conditional *Pinch1* KO (*Cnp*$^{Cre/+}$ *Pinch1*$^{flox/flox}$; *P1* cKO; b,f,j) and conditional *Pinch2* KO (*Cnp*$^{Cre/+}$ *Pinch2*$^{flox/flox}$; *P2* cKO; d,h,l) and the respective controls (CTR in a,e,i and c,g,k) at P30. Examples of axons with thicker myelin (white arrowheads) and myelin aberrations (red arrowheads) are indicated. Scale bars: 0.5 µm (ON and CC); 1 µm (SC). (B) *P2* cKOs had a lower *g*-ratio compared with the respective CTR. In contrast, no significant differences were found between *P1* cKO and CTR. Beeswarm superplots show the means per animal used to calculate the overall average, s.e.m. and *P*-values ($n$=3/5). At least 300 axons per animal were measured (dots). (C) Axon diameters were similar in *P2* cKO and CTR mice. At least 100 axons were measured (dots) per animal ($n$=3/5, larger symbols). (D) Periaxonal area was similar in *P2* cKO and CTR mice (ON). Mean value per animal (used to calculated the overall average and s.e.m.) is represented as a larger symbol in the beeswarm superplots ($n$=3/5). (E) Representative electron micrographs of cross-sections of ON and SC from *P2* cKO and CTR littermates at P90. Myelin outfoldings are identified by red arrowheads; other myelin redundant structures (whorls) are indicated by blue arrows. Scale bars: 0.5 µm, except for middle image of SC (1 µm). (F) Quantification of myelin outfolding profiles (CTR=1.30±0.22; *P2* cKO=4.15±0.55, $P$=0.0007) and myelin whorls (CTR=1.55±0.22; *P2* cKO=2.63±0.059; $P$=0.082) in ON ($n$=6). (G) Quantification of myelin outfolding profiles (CTR=3.85±1.09; *P2* cKO=9.47±1.42; $P$=0.024) and myelin whorls (CTR=2.70±0.66; *P2* cKO=8.60±2.55; $P$=0.048) in SC ($n$=3/4). (B-D,F,G) *$P\leq$0.05, ***$P\leq$0.001 (unpaired, two-tailed Student's *t*-test). (F,G) Error bars represent s.e.m.

Development (2022) 149, dev200597. doi:10.1242/dev.200597

myelinated axons from the ventral white matter of the SC of the cKOs showed that only the depletion of *Pinch2* resulted in thicker myelin sheaths (0.787±0.003 versus 0.750±0.013, $P$=0.049, $n$=3; Fig. S4D). We did not detect significant variations in the diameter of axons in ON (Fig. 3C, $P$=0.17, $n$=3/5), but the overall axonal diameters in SC were increased in *Pinch2* cKO compared with controls (1.43±0.06 versus 1.21±0.03, $P$=0.03, $n$=3) and displayed a tendency towards larger-caliber axons (Fig. S4E). This is in line with previous observations that point out that myelination increases axon caliber (Goebbels et al., 2010). We confirmed that myelin thickening was not caused by any variation in periaxonal compartments (Fig. 3D, $P$=0.97, $n$=3/5; Fig. S4G; 0.854±0.002 versus 0.828±0.007, $P$=0.040; $n$=3/5) (Goebbels et al., 2010) or changes in the periodicity of compact myelin lamellae ($P$=0.53, $n$=3; Fig. S4H), which supports the view that the thicker myelination resulted from extra myelin wraps. At P90, *g*-ratios did not differ significantly between *Pinch2* cKO and control (ON: $P$=0.32, $n$=3; SC: $P$=0.91, $n$=4/3; Fig. S4I), strongly suggesting the transient nature of the myelin phenotype in the ON and SC. The overall axon caliber average in the two regions was similar (ON: $P$=0.41, $n$=3; SC: $P$=0.42, $n$=4/3) despite the existence of a moderate increase in the numbers of larger caliber axons in cKO (Fig. S4J,K). Although the formation of aberrantly thick myelin sheaths can result from sustained activation of the Erk1/2 MAPK pathway (Ishii et al., 2013; Jeffries et al., 2016), this is likely not the case, as we did not detect significant changes in the levels of phosphor-Erk1/2 between *Pinch2* cKO and control nerves ($P$=0.76, $n$=3; Fig. S4L). In addition, the myelin overgrowth in *Pinch2* cKO is unlikely the result of hyperactivation of Akt (Flores et al., 2008) or negative regulation by PTEN (Goebbels et al., 2010) (Akt: $P$=0.36, $n$=3; PTEN: $P$=0.29, $n$=3; Fig. S4M,N).

The increase in the number of myelin sheaths – overmyelination – may result in focal hypermyelination or emergence of myelin abnormalities around myelinated axons. In addition to myelin overgrowth, electron microscopic analysis of ON, SC and CC at P30 also revealed the presence of redundant membrane outward loops (myelin outfoldings, indicated by red arrowhead in Fig. 3A,E, Fig. S5A) and isolated 'myelin-like' accumulations (myelin whorls, indicated by blue arrows in Fig. 3E, Fig. S5A) in *Pinch2* cKO. Although noticeable at P30 (Fig. S5A-C), morphometric analysis revealed that these myelin defects were significantly more abundant in P90 *Pinch2* cKO nerves compared with their age-matched controls ($P$=0.0007, $n$=6 in ON; $P$=0.024, $n$=3/4 in SC; Fig. 3F,G).

To eliminate the possibility that the loss of one *Cnp* allele per se was affecting the myelin ultrastructure, we quantified the frequency of myelin outfoldings and whorls in ultrathin sections of the SC from $Pinch2^{flox/wt}$ $Cnp^{Cre/+}$ mice and concluded that their frequency was similar to that in $Pinch2^{flox/flox}$ control mice ($P$=0.4, $n$=3; Fig. S5D, E). Together, these results strongly suggest that Pinch2-mediated signaling is required for normal myelination of CNS tracks.

Aberrant myelin profiles in the CNS are often associated with anomalous axoglial adhesion (Djannatian et al., 2019; Elazar et al., 2019). These contacts are essential to form paranodal axoglial junctions at the end of each myelin segment, where a cytoplasm-filled structure (or paranode loop) flanks the node of Ranvier. We examined paranode loops in longitudinal sections of the ON and ventral SC of P90 *Pinch2* cKO and control mice. Whereas in controls most of these structures were geometrically clustered at paranodes in an orderly fashion and contacted the axolemma (Fig. S5F, white arrowheads), in *Pinch2* cKOs these structures were often disorganized and did not establish appropriate contacts with the axon surface (white arrowheads). Defective contacts were better visualized at high magnification and we observed that in some paranodes the loops were piled up in disarray and often did not contact the axon but were positioned instead on top of compacted myelin. This was particularly evident in the outer loops (Fig. S5F, asterisks). We next measured the length of nodes of Ranvier in the SC and ON of *Pinch2* cKO and control adult mice (Fig. S5G, black dashed lines). Strikingly, we found that in both anatomical regions the node length was increased (0.79±0.03 versus 1.06±0.06, $P$=0.018, $n$=3 in SC; 0.83±0.03 versus 1.04±0.06, $P$=0.033, $n$=3 in ON) and distributed over a broader range in *Pinch2* cKO compared with controls (Fig. S5H,I). These alterations were not significantly correlated with either the node diameter or the axon diameter at the paranode (Fig. S5J-M).

These results suggest that OL-specific loss of *Pinch2* disrupts the node architecture potentially through the disintegration of essential axo-glia contacts, supporting a Pinch2-dependent function in myelin assembly and stability.

### Pinch2 regulates Rho GTPase activation

We and others previously showed that myelin formation depends on tight regulation of Rho GTPase-mediated signaling (Nodari et al., 2007; Pereira et al., 2009; Thurnherr et al., 2006; Benninger et al., 2007). Rho GTPases are molecular binary switches controlled by interchanging from an active guanosine triphosphate (GTP)-bound state into an inactive guanosine diphosphate (GDP)-bound form. They localize at focal adhesions (Legate et al., 2009) and are expressed in OLs (Liang et al., 2004; Erschbamer et al., 2005) where they are activated in a β1-integrin-dependent mode (Feltri et al., 2008). Ilk expression has also been shown to regulate Cdc42 and Rac1 activation in epithelial cells (Filipenko et al., 2005) and also in Schwann cells in the peripheral nervous system (Pereira et al., 2009). Rho GTPases regulate downstream targets that are directly associated with the dynamics of actin cytoskeleton reorganization, and local actin disassembly is fundamental in CNS myelin wrapping (Zuchero et al., 2015). We next examined the levels of classical Rho GTPases in ON lysates obtained from P30 cKO and control mice.

First, we measured RhoA activation levels using a rhotekin-GST fusion protein to pull down the activated form of RhoA in ON lysates. We found that the levels of the active GTP-bound form in *Pinch2* cKO ONs were significantly reduced compared with those in control ON (Fig. 4A,B; 1.38±0.079 versus 0.62±0.095, $P$=0.0036, $n$=3), whereas no significant changes were observed in the total amounts of RhoA (0.96±0.07 versus 1.04±0.06, $P$=0.4, $n$=3). To assess the *in vivo* relevance of our observations, we analyzed myelin ultrastructure in *Rhoa* cKO mice, obtained from crossing $Rhoa^{flox/flox}$ mice (Jackson et al., 2011) with $Cnp^{Cre/+}$ mice (Lappe-Siefke et al., 2003) (Fig. S6A). We found that at P25 *Rhoa* cKO ON contained axons with thicker myelin compared with controls (Fig. 4C,D; 0.817±0.004 versus 0.789±0.004, $P$=0.0096, $n$=3), suggesting that Ilk/Pinch2 signaling is required to activate RhoA and that suppression of RhoA activity elicits myelin growth. The overall size distribution of axonal dimeters was comparable in ONs of cKO and controls (Fig. S6B).

Remarkably, ablation of *Cdc42* in OL results in myelin abnormalities (Thurnherr et al., 2006) similar to those found here in the *Pinch2* cKO. Next, we measured the levels of active Cdc42 in ON from *Pinch2* cKO using a glutathione-S-transferase (GST)-PAK-CD protein fusion (Sander et al., 1998), in a similar manner to previous studies (Pereira et al., 2009; Benninger et al., 2007; Montani et al., 2014), and we found a significant decrease in the active form of Cdc42 (1.37±0.15 versus 0.73±0.10, $P$=0.025, $n$=3) in the mutant compared with the control (Fig. 5A,B) as well as in the

Development (2022) 149, dev200597. doi:10.1242/dev.200597

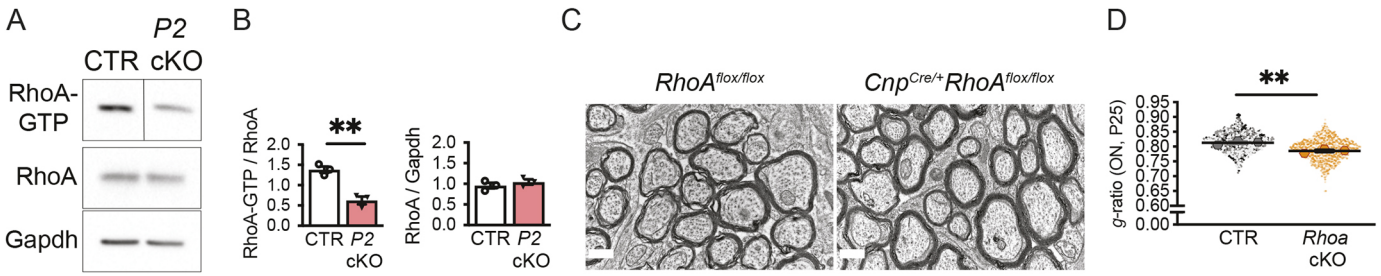


**Fig. 4. Downregulation of RhoA activity** and myelin overgrowth. (A) Pull-down assay for active GTP-bound RhoA in ON lysates from P30 *P2* cKO and control mice. (B) Quantification shows less active RhoA in *P2* cKO in comparison with control ($P$=0.004, $n$=3), and no significant changes in total RhoA expression ($n$=2 pooled nerves). **$P\leq$0.01 (unpaired, two-tailed Student's *t*-test). (C) Representative EM micrographs of cross-sections of ON from conditional *Rhoa* KO (*Cnp*$^{Cre/+}$*Rhoa*$^{flox/flox}$) and the respective control (*Rhoa*$^{flox/flox}$) at P25. Scale bars: 0.5 µm. (D) The *Rhoa* cKO displays a significantly lower *g*-ratio ($P$=0.0096, $n$=3). Beeswarm superplot shows mean per animal used to calculate the overall average, s.e.m. and *P*-value. **$P\leq$0.01 (unpaired, two-tailed Student's *t*-test). Dots represent individual measures per animal (minimum 176 myelinated axons).

active form of Rac1 in *Pinch2* cKO nerves (CTR=1.27±0.05; *P2* cKO=0.80±0.02; $P$=0.0002, Fig.S7A,B). In striking contrast, no significant changes were detected in *Pinch1* cKO nerves ($P$=0.20, $n$=6; Fig. S7C,D).

Cdc42 is involved in recruitment and oligomerization of cytoskeletal septins (Sadian et al., 2013), which form membrane-associated filaments (Bridges et al., 2014; Sirajuddin et al., 2007) assembly of which determines membrane binding and rigidity (Jiao et al., 2020; Gilden and Krummel, 2010). In myelin, septin filaments extend in the adaxonal compartment, thereby scaffolding mature myelin (Patzig et al., 2016). We found that the abundance of two of the most abundant septins in myelin, septins 2 and 8, was significantly reduced in myelin biochemically purified from the brains of *Cdc42* cKO mice compared with controls (Fig. 5C,D). Indeed, OL-specific ablation of *Sept8* causes the formation of myelin outfoldings (Patzig et al., 2016) similar to those seen in *Cdc42* mutants (Thurnherr et al., 2006) and *Pinch2* cKO. Therefore, we examined the expression of septins in protein lysates obtained from Pinch cKO ONs and respective controls. We found that Sept2 and Sept8 expression levels were significantly reduced in *Pinch2* cKO lysates compared with those from controls (Sept2: 0.73±0.02 versus 0.45±0.04, $P$=0.004, $n$=3/4; Sept8: 1.17±0.09 versus 0.67±0.10, $P$=0.002, $n$=3/4; Fig. 5E,F) and were not changed in age-matched *Pinch1* cKO nerves ($P$=0.87 and $P$=0.93, $n$=3); Fig. S7E,F).

Together, these results suggest that Pinch2-dependent regulation of Cdc42, via control of the assembly of the septin protein scaffold, underlie the establishment of structurally normal myelin.

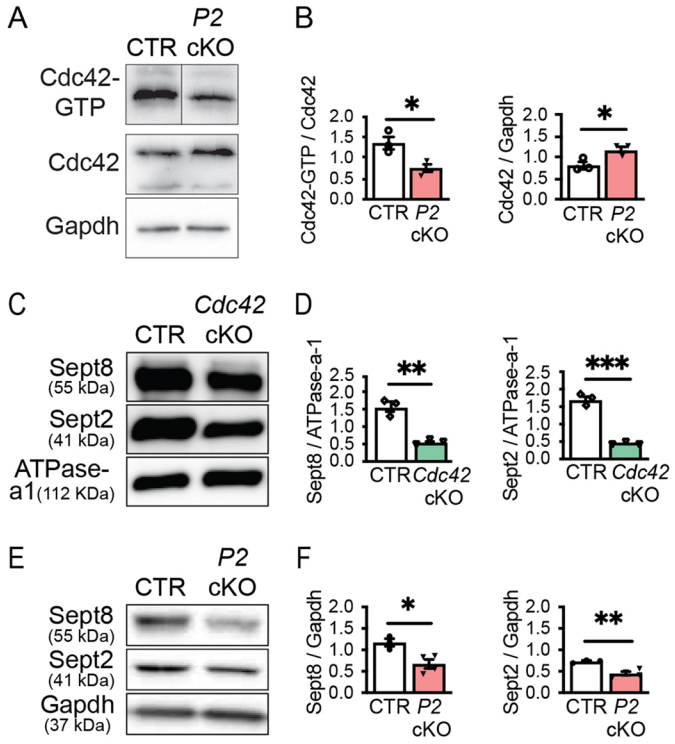


**Fig. 5. Cdc42 activation is deficient in the *Pinch2* cKO.** (A,B) Pull-down assay in lysates of *P2* cKO reveals a decrease in the active forms of Cdc4 ($P$=0.03, $n$=3) compared with CTR (P30). Total levels of Cdc42 relative to Gapdh show an increase in Cdc42 expression ($P$=0.04, $n$=3). Each *n* represents four pooled ONs. (C,D) The abundance of septins 8 and 2 is reduced in myelin purified from brains of *Cdc42* cKO mice at P45 (Sept8: $P$=0.004; Sept2: $P$=0.008; $n$=3). ATPase-a-1 was used as control. (E,F) Septins 8 and 2 are downregulated in ON from *P2* cKO (Sept8: $P$=0.02, $n$=3/4; Sept2: $P$=0.004, $n$=3/4). (B,D,F) *$P\leq$0.05, **$P\leq$0.01, ***$P\leq$0.001 (unpaired, two-tailed Student's *t*-test). Error bars represent s.e.m.

## DISCUSSION

In this study, we investigated the functions of Pinch1 and Pinch2 during developmental myelination using OL-targeted gene ablation in mice. Our data show that although one isoform can functionally compensate the loss of the other during early axon ensheathment, Pinch2 is essential for subsequent myelin wrapping. We found that loss of *Pinch2* leads to striking changes in myelin structure, including the formation of thicker myelin sheaths, the occurrence of myelin outfoldings, and alterations in paranodes and nodes of Ranvier. These myelin configurations emerge as the result of Pinch2 negative modulation of Rho GTPases, as suggested by the decrease in RhoA and Cdc42 activities and by the observation that the corresponding cKOs phenocopy, at least in part, the structural myelin alterations we observed in *Pinch2* cKO. Thus, our study supports the view of a bimodular arrangement of Pinch isoforms in the IPP complex as a defining aspect of OL function along development and shows for the first time that Pinch2 coordinates essential Rho GTP signaling in myelination (Fig. 6).

The possibility that the two Pinch proteins have partially redundant functions has been suggested before (Fukuda et al., 2003; Xu et al., 2005) but has never been formally demonstrated *in vivo*. Similar to other cell types, Pinch1 expression is detected earlier than Pinch2 in the developing OL. We found that the recruitment of either Pinch protein supports the integrity of the IPP complex during the initial stages of axon ensheathment and early myelination. Upon *Pinch1* loss and despite the absence of an obvious myelin phenotype, there is a transient increment of Olig2-positive cells

Development (2022) 149, dev200597. doi:10.1242/dev.200597

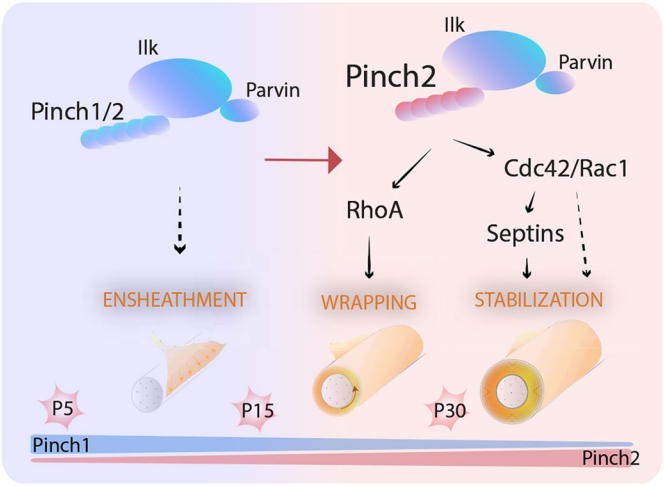


**Fig. 6. Ilk-Parvin-Pinch (IPP)-mediated signaling is required for the correct formation of myelin sheaths in the CNS.** Axon contact and ensheathment occurs in the presence of either Pinch isoform, but Pinch2 specifically controls myelin thickness and stability by modulating the activities of RhoA, Cdc42 and Rac1 Rho GTPases in the myelinating OL.

along with an increase in the expression of Erk1 and Erk2, known regulators OPC proliferation (Ishii et al., 2013). The increase in OPC number is balanced by augmented OL apoptosis likely through the transient activation of Jnk (Fig. S2) (Kadrmas et al., 2004), and is in line with the previously described pro-survival role of Pinch1 in the primitive endoderm (Montanez et al., 2012). This function of Pinch1 may rely on the binding to the Ras suppressor protein Rsu1, a negative regulator of Jnk signaling (Kadrmas et al., 2004) expressed in OLs (Zhang et al., 2014). Globally, this supports the involvement of Pinch1 in adjusting myelinating glia homeostasis during development. This capacity of the developing nervous system to counteract the initial excess of OLs (Raff et al., 1998) is thought to require integrin-mediated signaling (Benninger et al., 2006; Colognato et al., 2002; Laursen et al., 2009).

During development, Pinch2 protein expression is detected and peaks later than Pinch1 protein, which declines after the second postnatal week, when myelination in the ON progresses more intensely (Dangata and Kaufman, 1997; Foran and Peterson, 1992). At this stage, we observed a significant and progressive change in myelin structure (increase in the thickness of myelin sheath and in the emergence of myelin outfoldings) in *Pinch2* cKO mice. Thus, the developmentally driven increase in the abundance of Pinch2 and consequent change in the molecular composition of the IPP complex – IP(Pinch2) – appears to be essential for myelin formation and maturation.

Along with the obligatory binding partners Parvin and Ilk, Pinch proteins form the IPP protein complex, which bridges integrins and the actin cytoskeleton (Wickström et al., 2010; Legate et al., 2006). The tripartite IPP complex associates with various actin-binding proteins, including kindlin-2 (Fermt2) (Bledzka et al., 2016), paxillin and thymosin-B4 (Bock-Marquette et al., 2004) and Ilk protein regulates F-actin bundling through coordinated F-actin binding to Pinch1 and Parvin (Vaynberg et al., 2018). Depletion of α-Parvin (Montanez et al., 2009) or Ilk (Kogata et al., 2009) in mice vascular smooth muscle cells impair proper vessel formation by RhoA-mediated changes in actomyosin contractility. In the peripheral nervous system, loss of *Ilk* in Schwann cells results in upregulation of Rho/Rho kinase (ROCK) signaling and hampers the extension of cytoplasmic processes arresting radial sorting and, as a consequence, myelination (Pereira et al., 2009). Ilk regulates actin cytoskeleton dynamics and morphogenesis in OLs (O'Meara et al., 2013; Michalski et al., 2016). RhoA-elicited morphological changes and OL development have been studied *in vitro* (Liang et al., 2004; Wang et al., 2012; Rajasekharan et al., 2010) and support the view that OL process extension depends on the precise temporal modulation of active RhoA. Although it has previously been shown that actin filament assembly is initially required to form myelin segments in myelinating co-cultures (Azevedo et al., 2018), studies by Pedraza et al. indicated that inhibition of the RhoA downstream effector ROCK leads to enhanced formation of myelin segments in co-culture (Pedraza et al., 2014). This is in line with the observation that OL membrane spreading and myelin wrapping *in vivo* requires the loss of actin filaments as a result of the action of actin-severing and actin-depolymerization proteins (Zuchero et al., 2015; Nawaz et al., 2015). In the present work, we found a significant increase in the number of myelin wraps upon *Pinch2* depletion that was associated with a decrease in RhoA activity, suggesting that RhoA may be negatively controlling myelin sheath growth and preventing overmyelination. Because in *Pinch2* cKO nerves PI3K-AKT and PTEN signaling, known to drive myelin membrane growth (Harrington et al., 2010; Goebbels et al., 2010; Flores et al., 2008; Ishii et al., 2013), were not significantly affected, reduced RhoA activity could result in inhibition of actin nucleation via the Rho GTPase effectors Diaphanous-related formins (Kühn and Geyer, 2014), ultimately leading to a decrease of actin filaments and augmented membrane expansion and myelin wrapping. Of note, actin dynamics can also be controlled by Rsu1 protein (Kadrmas et al., 2004; Gonzalez-Nieves et al., 2013; Yang et al., 2021) and *Rsu1* transcript is reduced during OL development (Zhang et al., 2014) and in *Pinch2* cKOs (our results).

We and others have shown that cytoskeleton dynamics regulate different aspects of OL biology, including axonal wrapping and the proper formation of myelin sheaths (reviewed by Hughes and Appel, 2016; Domingues et al., 2018; Brown and Macklin, 2020). Analysis of the *Pinch2* cKO nerves also showed defects in paranodal axoglial junctions at the end of each internode (Fig. S5F) and in the length of the node of Ranvier (Fig. S5G-I) Changes in the length of the node of Ranvier may reflect an attempt to re-establish normal action potential conductance speed in response to myelin overgrowth. Increasing the length of the node could change capacitance and increase conduction speed along the nerve, potentially compensating for alterations in conduction along overmyelinated axons. This is in line with the notion that node of Ranvier length is a regulator of myelinated axon conductance in the CNS (Arancibia-Cárcamo et al., 2017). Flanking the nodes, the integrity of paranodes relies on integrin signaling (Laursen et al., 2009) and on axon-glia adhesions (Southwood et al., 2004), which, once dysregulated, could also result in abnormally thick myelin sheaths (Elazar et al., 2019).

Myelin outfoldings occur during normal development (Patzig et al., 2016; Snaidero et al., 2014) and are also a hallmark of age-dependent pathology in the CNS (Peters, 2002). In the mature CNS, an increased frequency of myelin outfoldings has been observed upon experimentally increasing phosphatidylinositol (3,4,5)-trisphosphate levels (Goebbels et al., 2010), changing actin organization and dynamics (Zuchero et al., 2015; Katanov et al., 2020) and septin assembly (Patzig et al., 2016; Erwig et al., 2019). *Pinch2* cKO, in which we observed a reduction in the pool of active Cdc42 (and Rac1; Fig. S7), displayed myelin outfoldings similar to those previously reported for OL-specific *Cdc42*/*Rac1* cKOs (Thurnherr et al., 2006). Importantly, *Cdc42*/*Rac1* cKOs do not

Development (2022) 149, dev200597. doi:10.1242/dev.200597

exhibit thicker myelin sheaths, which further supports the existence of an independent pathway limiting myelin wraps in *Pinch2* cKO.

Cdc42 has an essential role in the regulation of the assembly and disassembly of the septin complex, and the introduction of specific mutations in the budding yeast *Cdc42* gene that results in defective basal Cdc42 GTPase activity, leading to defective septin assembly (Gladfelter et al., 2002). This is consistent with our data showing reduced septin expression in *Cdc42* cKO ONs. Cdc42 GTPase negatively regulates the Borg proteins, which control the organization of septin network complex (Joberty et al., 2001). For example, Borg5 (also known as Cdc42ep1 and Cep1) is an effector of Cdc42 (Bagci et al., 2020) expressed in OLs (Zhang et al., 2014) and identified in myelin (Jahn et al., 2020). Filamentous septins were identified in the innermost layer of the myelin sheath assembled as longitudinal filaments in the non-compact adaxonal region of the membrane (Patzig et al., 2016). The assembly of the myelin septin filament correlates with myelin sheath stability, as suggested by the formation of myelin outfoldings when septin 8 is depleted (Patzig et al., 2016). Two subunits of the core myelin septin oligomer, septins 2 and 8, are significantly reduced in *Pinch2* cKO myelin. Because oligomer formation depends on the availability of individual septins (Hall et al., 2005), the decrease in Sept2 and Sept8 likely elicits the assembly of fewer oligomers and underlies the formation of myelin outfoldings in the *Pinch2* cKO similar to those found in the *Sept8* cKO (Patzig et al., 2016).

We note that *Pinch2* expression is increased during aging in the oligodendrocyte lineage (Ximerakis et al., 2019), which suggests a crucial role of Pinch2-mediated signaling with age. In aged non-diseased brains, the occurrence of myelin outfoldings (Peters, 2002; Patzig et al., 2016), similar to those observed in the *Pinch2* cKO (and the *Cdc42* cKO; Thurnherr et al., 2006), positively correlate with an age-associated decline in neurological function (Gunning-Dixon and Raz, 2000; Peters et al., 1996; Liu et al., 2017) and could reflect an increasingly less compliant cytoskeletal structure (Seixas et al., 2019) to maintain myelin stability. Hence, future studies on the IPP complex-mediated molecular mechanisms underlying the stabilization of myelin sheaths in the aging CNS could be particularly relevant to our understanding of age-associated systemic brain changes and cognitive impairment.

## MATERIALS AND METHODS

### Animals

Experiments were performed in strict compliance with the European Union Directive 2010/63/EU and the national Decreto-lei no. 113/2013. All protocols were approved by the local Ethical Committee and by the Portuguese Veterinarian Board (Licenses 2803/2021 and 24108/2013). Mice (*Mus musculus*) were co-housed in groups of up to six animals, fed with standard rodent diet and water *ad libitum* and kept in a 12 h light/dark cycle. Mice with floxed alleles for *Pinch1* (Li et al., 2005) (*Pinch1*$^{flox/flox}$ or *Pinch1*$^{flox/wt}$), *Pinch2* (Stanchi et al., 2005) (*Pinch2*$^{flox/flox}$ or *Pinch2*$^{flox/wt}$), *Rhoa* (Jackson et al., 2011) *Rhoa*$^{flox/flox}$ or *Rhoa*$^{flox/wt}$ and *Cdc42* (Wu et al., 2006) (*Cdc42*$^{flox/flox}$ or *Cdc42*$^{flox/wt}$) have been described previously. For OL-specific conditional depletion of *Pinch1*, *Pinch2*, *Cdc42* and *Rhoa*, mice carrying floxed alleles were crossed with the *Cnp-Cre* driver line (Lappe-Siefke et al., 2003). In all lines, experimental mice were on a C57BL/6 background. In the offspring, the relevant genotypes were determined by genomic PCR using the following primers: *Pinch1* forward 5′-CTAGGCTGGTAATGCAGGCC-3′ and reverse 5′-CCTGCCAATG-ATGAATTCAC-3′ [expected PCR product 230 bp (wt) and 400 bp (floxed)]; *Pinch2* forward 5′-CACTCCCAATTCCCCTCCCTGAG-3′ and reverse 5′-AGGGGTCTGAGGTCCTGAGAAGG-3′ [expected PCR product 298 bp (wt) and 438 bp (floxed)]; *Cdc42* forward 5′-TCTG-CCCTGATCTACACATACAC-3′ and reverse 5′-ATGTAGTGTCTGTC-CATTGG-3′ [expected PCR product 200 bp (wt) and 300 bp (floxed)]; *RhoA* forward 5′-AGCCAGCCTCTTGACCGATTTA-3′ and reverse 5′-TGTGGGATACCGTTTGAGCAT-3′ [expected PCR product 297 bp (wt) and 393 bp (floxed)]; *Cnp* forward 5′-GATGGGGCTTACTCTTGC-3′ and reverse 5′-CATAGCCTGAAGAACGAGA-3′ (expected PCR product 900 bp); *Cre* forward 5′-ACCAGGTTCGTTCACTCATGG-3′ and reverse 5′-AGGCTAAGTGCCTTCTCTACA-3′ (expected PCR product 230 bp). cKO genotypes are referred to as follows *Pinch1* cKO, *Pinch2* cKO, *Rhoa* cKO and *Cdc42* cKO. In all experimental setups, aged-matched males and females were arbitrarily used.

### Transcardial perfusion and tissue fixation

Adult mice were anesthetized by terminal intraperitoneal administration of pentobarbital (0.2 ml/30 g body weight) and subsequently transcardially perfused with sterile, filtered and pre-warmed at 37°C PBS or 0.1 M phosphate buffer (PB) pH 7.4, depending on whether the dissection of specimens was for regular histology or to be used in electron microscopy (EM). This was immediately followed by pre-warmed (37°C) fixative perfusion, using 4% paraformaldehyde solution prepared in PBS (samples for immunocytochemistry), or 4% paraformaldehyde/3% glutaraldehyde solution prepared in PB (samples for EM). After dissection, the tissue of interest for immunohistochemistry was incubated overnight in 4% paraformaldehyde in PBS, and then immersed in sterile 20% (w/v) sucrose in PBS until tissue reached the bottom of the reservoir for optimal tissue infiltration. Fixed samples were embedded in Cryomatrix embedding medium (Fisher Scientific, 6769006), and stored at −80°C. Samples used in EM were postfixed at least overnight in the fixative solution.

### TEM

White matter samples were visualized using TEM in perfusion fixed tissue. P15, young adult (P30) or adult (P90) were fixed by cardiac perfusion with 4% paraformaldehyde/3% glutaraldehyde in 0.1 M PB, pH 7.4. After dissection, the relevant regions from the CNS (ON, thoracic SC, CC) were left in perfusing buffer for at least 12 h, and then postfixed overnight in 1% osmium tetroxide in 0.1 M PB. Samples were then dehydrated through increasing ethanol concentrations and finally resin-embedded. Control and KO material were handled in parallel to avoid misinterpretation of myelin changes and the discard of myelin artifacts. Blocks were processed in a ultramicrotome to obtain 1 µm-thick sections (thin sections), which were stained with Toluidine Blue to assess the integrity of samples and to select further the tissue for analysis. Next, 60 nm-thick sections (ultrathin sections) from the selected areas were cut, counterstained using 3% uranyl acetate and 1% lead citrate, transferred onto slotted grids and visualized using a Jeol JEM 1400 electron microscope at 80 Kv, coupled to an Orius Gatan camera. Standard hexagonal mesh grids were used, except when larger samples were imaged for quantification purposes. In this case, single hole grids coated with pioloform (0.7% in chloroform solution) were used. At least three animals per genotype were visualized. To obtain representative high-resolution images, ultrathin sections were imaged, typically at 25,000×, 12,000× and 30,000× for ON, SC and CC, respectively. For quantifications, images were taken at 12,000×. Image processing was performed using ImageJ 1.52h (Schindelin et al., 2012) and Photoshop CS5.

### Quantification and morphometric analysis

Both males and females were used in the study. All the quantifications were performed with the researcher(s) blind to the genotypes of the mice. For EM, randomly digitized and non-overlapping images of the ON or ventral SC were analyzed for *g*-ratios by measuring at least 100 axons per animal. In order to identify contacted axons (P15), 6% overlapping images from half of the ON were stitched (Photomerge, Photoshop). For western blots, the results were compared preferentially among the same membrane blot and, if possible, using animals from the same litter (the rare cases where this was not possible are stated in the text). Bands were quantified using Image Lab, except for comparisons among different membranes (Fiji). In either case, blots displaying areas of the bands with saturated signal intensity (above a measurable range at Image Lab) were discarded.

For morphological analysis (*g*-ratios) on ultrathin sections, at least ten images per animal were randomly taken at 12,000×. *G*-ratios were calculated by dividing the area of the axon, inferred from the measured perimeter, by

Development (2022) 149, dev200597. doi:10.1242/dev.200597

the area of fiber (axon with myelin), also inferred from the measured perimeter. At least 100 axons were measured from at least three animals per genotype. At P30, we used an alternative method in parallel, so that the diameter of compacted myelin (replacing axon diameter), was divided by the outer diameter of the myelin sheath (Goebbels et al., 2010). To determine the number of contacted/myelinated axons in the ON, quantification was carried after image alignment (Photoshop CS6) from a hemisection of the ON (P15). To quantify myelin outfolding profiles: 741-1000 (Fig. 3E), 397-849 (Fig. 3F), 1600 (Fig. S5B), 320 (Fig. S5C) and 450 (Fig. S5E) were examined in at least ten random and non-overlapping frames per animal (12,000 EM images). To quantify the length of nodes of Ranvier and the diameter of nodes and axons at the node (Fig. S5J-M), 75-87 axons of the SC and 47-81 axons of the ON per genotype were examined. Every quantification involving EM images was performed manually using ImageJ.

### Western blotting

For protein analysis, the indicated region of the CNS were dissected and immediately frozen. The frozen tissue was homogenized using a chilled micropestle in cold RIPA buffer (Sigma-Aldrich, R0278), supplemented with 1 mM EDTA and protease and phosphatase inhibitors, according to the manufacturer's instructions. Samples were cleared in a pre-cooled centrifuge for 30 min at 4°C under maximum speed (17,000 ***g***). For optic tissue, and unless stated, two nerves from one animal were loaded per lane. For SC, protein concentration was measured using the colorimetric BCA Protein assay (Pierce, 23225) and 10 µg of protein per lane were resolved in 10% or 12% SDS-polyacrylamide gels, after dilution in gel loading buffer (GLB; 150 mM Trizma Base, 6% SDS, 0.05% Bromophenol Blue, 30% glycerol, 6 mM EDTA pH 8.8) and freshly added DTT (1 mM). Heat-induced denaturation of proteins was achieved by a 10 min incubation at 95°C immediately before loading. The pre-stained marker Precision Plus Protein Dual Color Standard (Bio-Rad) was used to determine approximate molecular weights and monitor transfer efficiency. Before blocking, protein bands were visualized by Ponceau S staining. For the immunoblots displayed in Fig. 5E, myelin was purified from the brains of mice as previously reported (Patzig et al., 2016) and separated on 10% gels with a protein load of 5 µg per lane (Sept2) or 10 µg per lane (Sept8, ATP1A1). Instead of heat denaturation, samples were incubated for 10 min at 42°C before loading. Nitrocellulose membranes were blocked for 1 h in 5% nonfat dry milk in TBS-Tween (TBS-T) or 90 min in 5% bovine serum albumin (BSA)-TBS-T. Incubation with primary antibodies in blocking solution overnight, with rotation at 4°C, was followed by membrane washing with TBS-T for 30 min and incubation with horseradish peroxidase-conjugated secondary antibodies at room temperature. After washing, blots were incubated with SuperSignal West Pico Chemiluminescent Substrate (Thermo Fisher Scientific) reagent for band detection and the signal was detected using a ChemiDoc Imaging System (XRS, Bio-Rad) coupled to ImageLab software.

### Immunostaining

Paraformaldehyde (4%)-fixed samples of *Pinch1* cKO or *Pinch2* cKO and the respective controls were cut in 14 µm thin cross-sections using a Leica CM 3050S cryostat. KOs and the respective control animals were always transferred to the same slide (SuperFrost Plus-coated slides). To minimize bias in processing the tissues, 5-12 sections per animal were transferred to a slide, and simultaneously processed before being subjected to blinded analysis. For fluorescence staining, sections were rinsed in TBS for 10 min, permeabilized with 0.5% Triton X-100 in TBS for 15 min and blocked for 1 h in blocking solution (10% normal goat serum, 1% BSA, 0.025% Triton X-100 in TBS). Samples were then incubated overnight at 4°C in 1% BSA and 0.025% Triton X-100 in TBS. After washing three times with 0.025% Triton X-100 in TBS (TBS-T) for 15 min, samples were incubated with the secondary antibody for at least 1 h in TBS with 1% BSA at room temperature. The samples on the slide were washed with TBS-T, incubated with 4′,6-diamidino-2-phenylindole (DAPI, Sigma-Aldrich) for 10 min, washed again with TBS-T, and left to dry prior to imaging. Slides were mounted using Fluoroshield (Sigma-Aldrich) and left to dry prior to imaging.

### Antibodies

Antibodies against Pinch proteins were raised using C-terminal-based peptides for immunization: CLKKLSETLGRK for Pinch1 and CAQPKSVDVNSL for Pinch2 (Li et al., 2005). The antibodies detected Pinch1 or Pinch2 at the estimated apparent molecular weights on a western blot, at 1:1000 under standard denaturing conditions. Other primary antibodies used in western blot analysis were: Ilk (BD Biosciences, 611803, 1:1000), α-Parvin (Abcam, 11336, 1:3000), Akt (Cell Signaling Technology, 9272, 1:1000), p-Akt Thr 308 (Cell Signaling Technology, 2965, 1:1000), p38 (Cell Signaling Technology, 8690, 1:1000), p-p38 (Cell Signaling Technology, 4511, 1:1000), Erk (Cell Signaling Technology, 9102, 1:1000), p-Erk (Cell Signaling Technology, 9101, 1:1000), Jnk (Cell Signaling Technology, 9258, 1:1000), p-Jnk (Cell Signaling Technology 4668, 1:1000), Pten (Cell Signaling Technology, 9188, 1:1000), Sept8 (Proteintech, 11769-1-AP, 1:2500), Sept2 (Proteintech, 11397-1-AP, 1:500), ATP1A1 (Abcam, ab7671, 1:2500), Cdc42 (Cell Signaling Technology, 2466, 1:1000), RhoA (67B9) (Cell Signaling Technology, 2117, 1:1000), Gapdh (HyTest, 6C5, 1:50,000), α-tubulin (Sigma-Aldrich, T5168, 1:10,000). Either Gapdh or α-tubulin were used as reference to avoid superimposed bands in blots. Peroxidase-conjugated AffiniPure donkey anti-rabbit IgG (Jackson ImmunoResearch, 711-035-152. 1:10000), peroxidase-conjugated AffiniPure goat anti-mouse IgG (Jackson ImmunoResearch, 115-035-146, 1:15000), peroxidase-conjugated AffiniPure goat anti-rat IgG (Jackson ImmunoResearch, 112-035-003, 1:10000) were used as secondary antibodies for western blot.

All these antibodies were used in standard conditions (blocking and antibody incubations in 5% low fat milk in TBS-T), except the antibodies for Cdc42 and for the phosphorylated forms of the proteins, which were incubated in 5% BSA in TBS-T.

For immunostaining, the following primary antibodies were used: Olig2 (Millipore, AB9610, 1:500) and CC1 (Calbiochem, OP80, 1:200). Alexa Fluor 488 anti-rabbit (Alfagene, A11008, 1.1000) and Cy3-conjugated AffiniPure goat anti-mouse IgG (Jackson ImmunoResearch, 115-165-146, 1:1000) were used as secondary antibodies.

### Rho GTPase activity assay

RhoA and Cdc42 activities were measured using either a GST-rhotekin or PAK-CD (PAK-CRIB domain)-based assay, as described previously (Sander et al., 1998; Manser et al., 1994). Briefly, expression of recombinant protein GS-rhotekin or GST-PAK-CD was induced in transformed BL21 *Escherichia coli* by addiction of 0.1 M isopropylthiogalactoside for 4 h. After harvesting, bacteria were resuspended in lysis buffer (50 mM Tris-HCl, pH 8.2, mM $MgCl_2$, 0.2 mM $Na_2S_2O$, 10% glycerol, 20% sucrose, 2 mM dithiothreitol, 1 µg/ml leupeptin, 1 µg/ml pepstatin and 1 µg/ml aprotinin) and sonicated at 4°C. Cell lysates were centrifuged for 20 min at 4°C (45,000 ***g***) and the cleared supernatant stored at −80°C. For bait immobilization, 300 µl of supernatant was incubated with 40 µl of Glutathione High Capacity magnetic agarose beads (Sigma-Aldrich) for at least 30 min, at 4°C, with gentle agitation. Beads were washed twice using lysis buffer and twice with FISH buffer (10% glycerol, 50 mM Tris-HCl, pH 7.4, 100 mM NaCl, 1% NP-40, 2 mM $MgCl_2$). A second tube was subjected to the same steps containing equivalent volumes of beads and FISH buffer (instead of bait). The contents of the two tubes (bait-immobilized beads and 'clean' beads) was mixed and then evenly distributed in two tubes with lysates. To prepare the lysates, the ONs from at least two animals (P30) were pooled, homogenized in cold FISH buffer (with protease inhibitor cocktail) and centrifuged for 15 min at 4°C (13,000 ***g***). Exactly 10% of the volume was taken and frozen (input). The remaining supernatant was incubated with the bacterially produced GST-rhotekin or GST-PAK-CD fusion bound to GST-coupled magnetic beads for about 12 h, with gentle agitation at 4°C, and washed four times with excess of FISH buffer with cocktail of protease inhibitors). For elution, GLB was added and samples were incubated at 95°C for 10 min. Samples were resolved on a 12% SDS PAGE gel (pull-down samples run between empty lanes), followed by standard western blot and Ponceau S staining to confirm uniform pull-downs prior to detection with the relevant antibodies.

### Statistical analysis

Assumptions on normality were made based on prior testing of Gaussian distribution using the Shapiro–Wilk test. Homogeneity of variances were assumed to be identical, but whenever this assumption was not met (F-test for equality of two variances, $P>0.05$), the Student's *t*-test was replaced by the non-parametric Mann–Whitney *U*-test to compare two independent groups on a continuous outcome. Statistical analyses were performed using GraphPad Prism version 8.3.1 (RRID: SCR_002798) for Mac OS. Unless otherwise stated and in cases when only two conditions or samples (e.g. genotypes) were compared, data were analyzed by unpaired, two-tailed Student's *t*-test. Multiple group analysis was performed using one-way ANOVA and post-hoc tests as indicated in figure legends. Further analyses are described in the legends of the figures. All controls and KO mice were littermates, and often sample size corresponds to the litter size and to the numbers generally employed in the field, although no statistical method was employed for sample size determination. Outliers were not excluded and all data are expressed as mean±s.e.m. to describe the variability within at least three independent samples. Scatter SuperPlots (Lord et al., 2020) were specifically designed to convey experimental variability, in which the full dataset of technical replicates was overlaid with a second plot with the corresponding averages of biological replicates (in Figs 2C, 3B-D, 4D).

#### Acknowledgements

We thank K.-A. Nave (Max Planck Institute of Experimental Medicine, Göttingen) for the *Cnp-Cre* transgenic line and M. S. Erwig (Max Planck Institute of Experimental Medicine, Göttingen) for technical assistance. We acknowledge Ana Seixas (i3S, Porto) for insightful observations and critic revision of the manuscript, and Jorge A. Pereira (ETH, Switzerland) and Huiliang Li (UCL, UK) for helpful discussions and critical revision of the manuscript. We thank technical support from i3S scientific platforms Histology and Electron Microscopy and Advanced Light Microscopy (members of the national infrastructure PPBI-Portuguese Platform of BioImaging, supported by POCI-01-0145-FEDER-022122), and the Cell Culture and Genotyping and the Animal Facilities.

#### Competing interests

The authors declare no competing or financial interests.

#### Author contributions

Conceptualization: J.P.d.F., J.B.R.; Methodology: J.P.d.F., R.S.V.-S., H.B.W.; Validation: J.P.d.F.; Formal analysis: J.P.d.F., R.S.V.-S.; Investigation: J.P.d.F., R.S.V.-S.; Resources: J.P.d.F.; Data curation: J.P.d.F., R.S.V.-S.; Writing - original draft: J.P.d.F.; Writing - review & editing: J.P.d.F., R.F., H.B.W., J.B.R.; Visualization: J.P.d.F.; Supervision: J.P.d.F., J.B.R.; Project administration: J.P.d.F., J.B.R.; Funding acquisition: J.B.R.

#### Funding

This work was financially supported by Fundo Europeu de Desenvolvimento Regional (FEDER; European Regional Development Fund) funds through the COMPETE 2020 Operacional Programme for Competitiveness and Internationalisation (POCI), Portugal 2020, and by Portuguese funds through FCT (Fundação para a Ciência e a Tecnologia)/Ministério da Ciência, Tecnologia e Ensino Superior in the framework of the project POCI-01-0145-FEDER-031318989 (PTDC/MED-NEU/31318/2017). H.B.W is supported by the Deutsche Forschungsgemeinschaft (German Research Foundation; WE2720/2-2). J.P.d.F. and R.S.V.-S. are funded by national funds through FCT (J.P.d.F.: SFRH/BPD/113359/2015, program-contract described in paragraphs 4, 5, and 6 of art. 23 of Law no. 1001 57/ 2016, of August 29, as amended by Law no. 57/2017 of July 2019; R.V.S.: SFRH/BD/145744/2019).

#### Data availability

Datasets available online (Dryad). Raw data are available online at Zenodo (https://zenodo.org/) under accession number 6723849.

#### Peer review history

The peer review history is available online at https://journals.biologists.com/dev/article-lookup/doi/10.1242/dev.200597.

#### References

**Arancibia-Cárcamo, I. L., Ford, M. C., Cossell, L., Ishida, K., Tohyama, K. and Attwell, D.** (2017). Node of Ranvier length as a potential regulator of myelinated axon conduction speed. *Elife* **6**, e23329. doi:10.7554/eLife.23329

**Azevedo, M. M., Domingues, H. S., Cordelières, F. P., Sampaio, P., Seixas, A. I. and Relvas, J. B.** (2018). Jmy regulates oligodendrocyte differentiation via modulation of actin cytoskeleton dynamics. *Glia* **66**, 1826-1844. doi:10.1002/glia.23342

**Bagci, H., Sriskandarajah, N., Robert, A., Boulais, J., Elkholi, I. E., Tran, V., Lin, Z.-Y., Thibault, M.-P., Dubé, N., Faubert, D. et al.** (2020). Mapping the proximity interaction network of the Rho-family GTPases reveals signalling pathways and regulatory mechanisms. *Nat. Cell Biol.* **22**, 120-134. doi:10.1038/s41556-019-0438-7

**Benninger, Y., Colognato, H., Thurnherr, T., Franklin, R. J., Leone, D. P., Atanasoski, S., Nave, K. A., Ffrench-Constant, C., Suter, U. and Relvas, J. B.** (2006). β1-integrin signaling mediates premyelinating oligodendrocyte survival but is not required for CNS myelination and remyelination. *J. Neurosci.* **26**, 7665-7673. doi:10.1523/JNEUROSCI.0444-06.2006

**Benninger, Y., Thurnherr, T., Pereira, J. A., Krause, S., Wu, X., Chrostek-Grashoff, A., Herzog, D., Nave, K.-A., Franklin, R. J., Meijer, D. et al.** (2007). Essential and distinct roles for cdc42 and rac1 in the regulation of Schwann cell biology during peripheral nervous system development. *J. Cell Biol.* **177**, 1051-1061. doi:10.1083/jcb.200610108

**Bledzka, K., Bialkowska, K., Sossey-Alaoui, K., Vaynberg, J., Pluskota, E., Qin, J. and Plow, E. F.** (2016). Kindlin-2 directly binds actin and regulates integrin outside-in signaling. *J. Cell Biol.* **213**, 97-108. doi:10.1083/jcb.201501006

**Bock-Marquette, I., Saxena, A., White, M. D., Dimaio, J. M. and Srivastava, D.** (2004). Thymosin β4 activates integrin-linked kinase and promotes cardiac cell migration, survival and cardiac repair. *Nature* **432**, 466-472. doi:10.1038/nature03000

**Braun, A., Bordoy, R., Stanchi, F., Moser, M., Kostka, G. G., Ehler, E., Brandau, O. and Fässler, R.** (2003). PINCH2 is a new five LIM domain protein, homologous to PINCHand localized to focal adhesions. *Exp. Cell Res.* **284**, 239-250. doi:10.1016/S0014-4827(02)00039-3

**Bridges, A. A., Zhang, H., Mehta, S. B., Occhipinti, P., Tani, T. and Gladfelter, A. S.** (2014). Septin assemblies form by diffusion-driven annealing on membranes. *Proc. Natl. Acad. Sci. USA* **111**, 2146-2151. doi:10.1073/pnas.1314138111

**Brown, T. L. and Macklin, W. B.** (2020). The actin cytoskeleton in myelinating cells. *Neurochem. Res.* **45**, 684-693. doi:10.1007/s11064-019-02753-0

**Chun, S. J., Rasband, M. N., Sidman, R. L., Habib, A. A. and Vartanian, T.** (2003). Integrin-linked kinase is required for laminin-2-induced oligodendrocyte cell spreading and CNS myelination. *J. Cell Biol.* **163**, 397-408. doi:10.1083/jcb.200304154

**Colognato, H., Baron, W., Avellana-Adalid, V., Relvas, J. B., Baron-Van Evercooren, A., Georges-Labouesse, E. and Ffrench-Constant, C.** (2002). CNS integrins switch growth factor signalling to promote target-dependent survival. *Nat. Cell Biol.* **4**, 833-841. doi:10.1038/ncb865

**Dangata, Y. Y. and Kaufman, M. H.** (1997). Myelinogenesis in the optic nerve of (C57BL x CBA) F1 hybrid mice: a morphometric analysis. *Eur. J. Morphol.* **35**, 3-17. doi:10.1076/ejom.35.1.3.13057

**Djannatian, M., Timmler, S., Arends, M., Luckner, M., Weil, M. T., Alexopoulos, I., Snaidero, N., Schmid, B., Misgeld, T., Möbius, W. et al.** (2019). Two adhesive systems cooperatively regulate axon ensheathment and myelin growth in the CNS. *Nat. Commun.* **10**, 4794. doi:10.1038/s41467-019-12789-z

**Domingues, H. S., Cruz, A., Chan, J. R., Relvas, J. B., Rubinstein, B. and Pinto, I. M.** (2018). Mechanical plasticity during oligodendrocyte differentiation and myelination. *Glia* **66**, 5-14. doi:10.1002/glia.23206

**Dougherty, G. W., Chopp, T., Qi, S.-M. and Cutler, M. L.** (2005). The Ras suppressor Rsu-1 binds to the LIM 5 domain of the adaptor protein PINCH1 and participates in adhesion-related functions. *Exp. Cell Res.* **306**, 168-179. doi:10.1016/j.yexcr.2005.01.025

**Eke, I., Koch, U., Hehlgans, S., Sandfort, V., Stanchi, F., Zips, D., Baumann, M., Shevchenko, A., Pilarsky, C., Haase, M. et al.** (2010). PINCH1 regulates Akt1 activation and enhances radioresistance by inhibiting PP1α. *J. Clin. Invest.* **120**, 2516-2527. doi:10.1172/JCI41078

**Elazar, N., Vainshtein, A., Golan, N., Vijayaragavan, B., Schaeren-Wiemers, N., Eshed-Eisenbach, Y. and Peles, E.** (2019). Axoglial adhesion by Cadm4 regulates CNS myelination. *Neuron* **101**, 224-231.e5. doi:10.1016/j.neuron.2018.11.032

**Erschbamer, M. K., Hofstetter, C. P. and Olson, L.** (2005). RhoA, RhoB, RhoC, Rac1, Cdc42, and Tc10 mRNA levels in spinal cord, sensory ganglia, and corticospinal tract neurons and long-lasting specific changes following spinal cord injury. *J. Comp. Neurol.* **484**, 224-233. doi:10.1002/cne.20471

**Erwig, M. S., Patzig, J., Steyer, A. M., Dibaj, P., Heilmann, M., Heilmann, I., Jung, R. B., Kusch, K., Mobius, W., Jahn O. et al.** (2019). Anillin facilitates septin assembly to prevent pathological outfoldings of central nervous system myelin. *eLife*, **8**. doi:10.7554/eLife.43888

**Feltri, M. L., Suter, U. and Relvas, J. B.** (2008). The function of RhoGTPases in axon ensheathment and myelination. *Glia* **56**, 1508-1517. doi:10.1002/glia.20752

**Feltri, M. L., Poitelon, Y. and Previtali, S. C.** (2016). How schwann cells sort axons: new concepts. *Neuroscientist* **22**, 252-265. doi:10.1177/1073858415572361

**Filipenko, N. R., Attwell, S., Roskelley, C. and Dedhar, S.** (2005). Integrin-linked kinase activity regulates Rac- and Cdc42-mediated actin cytoskeleton reorganization via alpha-PIX. *Oncogene* **24**, 5837-5849. doi:10.1038/sj.onc.1208737

**Flores, A. I., Mallon, B. S., Matsui, T., Ogawa, W., Rosenzweig, A., Okamoto, T. and Macklin, W. B.** (2000). Akt-mediated survival of oligodendrocytes induced by

neuregulins. *J. Neurosci.* **20**, 7622-7630. doi:10.1523/JNEUROSCI.20-20-07622.2000

**Flores, A. I., Narayanan, S. P., Morse, E. N., Shick, H. E., Yin, X., Kidd, G., Avila, R. L., Kirschner, D. A. and Macklin, W. B.** (2008). Constitutively active Akt induces enhanced myelination in the CNS. *J. Neurosci.* **28**, 7174-7183. doi:10.1523/JNEUROSCI.0150-08.2008

**Foran, D. R. and Peterson, A. C.** (1992). Myelin acquisition in the central nervous system of the mouse revealed by an MBP-Lac Z transgene. *J. Neurosci.* **12**, 4890-4897. doi:10.1523/JNEUROSCI.12-12-04890.1992

**Fukuda, T., Chen, K., Shi, X. and Wu, C.** (2003). PINCH-1 is an obligate partner of integrin-linked kinase (ILK) functioning in cell shape modulation, motility, and survival. *J. Biol. Chem.* **278**, 51324-51333. doi:10.1074/jbc.M309122200

**Gilden, J. and Krummel, M. F.** (2010). Control of cortical rigidity by the cytoskeleton: emerging roles for septins. *Cytoskeleton* **67**, 477-486. doi:10.1002/cm.20461

**Gladfelter, A. S., Bose, I., Zyla, T. R., Bardes, E. S. and Lew, D. J.** (2002). Septin ring assembly involves cycles of GTP loading and hydrolysis by Cdc42p. *J. Cell Biol.* **156**, 315-326. doi:10.1083/jcb.200109062

**Goebbels, S., Oltrogge, J. H., Kemper, R., Heilmann, I., Bormuth, I., Wolfer, S., Wichert, S. P., Mobius, W., Liu, X., Lappe-Siefke, C. et al.** (2010). Elevated phosphatidylinositol 3,4,5-trisphosphate in glia triggers cell-autonomous membrane wrapping and myelination. *J. Neurosci.* **30**, 8953-8964. doi:10.1523/JNEUROSCI.0219-10.2010

**Gonzalez-Nieves, R., Desantis, A. I. and Cutler, M. L.** (2013). Rsu1 contributes to regulation of cell adhesion and spreading by PINCH1-dependent and -independent mechanisms. *J. Cell Commun. Signal* **7**, 279-293. doi:10.1007/s12079-013-0207-5

**Gunning-Dixon, F. M. and Raz, N.** (2000). The cognitive correlates of white matter abnormalities in normal aging: a quantitative review. *Neuropsychology* **14**, 224-232. doi:10.1037/0894-4105.14.2.224

**Guo, L., Wang, R., Zhang, K., Yuan, J., Wang, J., Wang, X., Ma, J. and Wu, C.** (2019). A PINCH-1-Smurf1 signaling axis mediates mechano-regulation of BMPR2 and stem cell differentiation. *J. Cell Biol.* **218**, 3773-3794. doi:10.1083/jcb.201902022

**Hall, P. A., Jung, K., Hillan, K. J. and Russell, S. E.** (2005). Expression profiling the human septin gene family. *J. Pathol.* **206**, 269-278. doi:10.1002/path.1789

**Harrington, E. P., Zhao, C., Fancy, S. P., Kaing, S., Franklin, R. J. and Rowitch, D. H.** (2010). Oligodendrocyte PTEN is required for myelin and axonal integrity, not remyelination. *Ann. Neurol.* **68**, 703-716. doi:10.1002/ana.22090

**Hobert, O., Moerman, D. G., Clark, K. A., Beckerle, M. C. and Ruvkun, G.** (1999). A conserved LIM protein that affects muscular adherens junction integrity and mechanosensory function in Caenorhabditis elegans. *J. Cell Biol.* **144**, 45-57. doi:10.1083/jcb.144.1.45

**Hughes, E. G. and Appel, B.** (2016). The cell biology of CNS myelination. *Curr. Opin. Neurobiol.* **39**, 93-100. doi:10.1016/j.conb.2016.04.013

**Hussain, R. and Macklin, W. B.** (2017). Integrin-linked kinase (ILK) deletion disrupts oligodendrocyte development by altering cell cycle. *J. Neurosci.* **37**, 397-412. doi:10.1523/JNEUROSCI.2113-16.2016

**Ishii, A., Furusho, M. and Bansal, R.** (2013). Sustained activation of ERK1/2 MAPK in oligodendrocytes and schwann cells enhances myelin growth and stimulates oligodendrocyte progenitor expansion. *J. Neurosci.* **33**, 175-186. doi:10.1523/JNEUROSCI.4403-12.2013

**Jackson, B., Peyrollier, K., Pedersen, E., Basse, A., Karlsson, R., Wang, Z., Lefever, T., Ochsenbein, A. M., Schmidt, G., Aktories, K. et al.** (2011). RhoA is dispensable for skin development, but crucial for contraction and directed migration of keratinocytes. *Mol. Biol. Cell* **22**, 593-605. doi:10.1091/mbc.e09-10-0859

**Jahn, O., Siems, S. B., Kusch, K., Hesse, D., Jung, R. B., Liepold, T., Uecker, M., Sun, T. and Werner, H. B.** (2020). The CNS myelin proteome: deep profile and persistence after post-mortem delay. *Front. Cell Neurosci.* **14**, 239. doi:10.3389/fncel.2020.00239

**Jeffries, M. A., Urbanek, K., Torres, L., Wendell, S. G., Rubio, M. E. and Fyffe-Maricich, S. L.** (2016). ERK1/2 activation in preexisting oligodendrocytes of adult mice drives new myelin synthesis and enhanced CNS function. *J. Neurosci.* **36**, 9186-9200. doi:10.1523/JNEUROSCI.1444-16.2016

**Jiao, F., Cannon, K. S., Lin, Y.-C., Gladfelter, A. S. and Scheuring, S.** (2020). The hierarchical assembly of septins revealed by high-speed AFM. *Nat. Commun.* **11**, 5062. doi:10.1038/s41467-020-18778-x

**Joberty, G., Perlungher, R. R., Sheffield, P. J., Kinoshita, M., Noda, M., Haystead, T. and Macara, I. G.** (2001). Borg proteins control septin organization and are negatively regulated by Cdc42. *Nat. Cell Biol.* **3**, 861-866. doi:10.1038/ncb1001-861

**Kadrmas, J. L., Smith, M. A., Clark, K. A., Pronovost, S. M., Muster, N., Yates, J. R., 3rd. and Beckerle, M. C.** (2004). The integrin effector PINCH regulates JNK activity and epithelial migration in concert with Ras suppressor 1. *J. Cell Biol.* **167**, 1019-1024. doi:10.1083/jcb.200408090

**Katanov, C., Novak, N., Vainshtein, A., Golani, O., Dupree, J. L. and Peles, E.** (2020). N-Wasp regulates oligodendrocyte myelination. *J. Neurosci.* **40**, 6103-6111. doi:10.1523/JNEUROSCI.0912-20.2020

**Kogata, N., Tribe, R. M., Fässler, R., Way, M. and Adams, R. H.** (2009). Integrin-linked kinase controls vascular wall formation by negatively regulating Rho/ROCK-mediated vascular smooth muscle cell contraction. *Genes Dev.* **23**, 2278-2283. doi:10.1101/gad.535409

**Kühn, S. and Geyer, M.** (2014). Formins as effector proteins of Rho GTPases. *Small GTPases* **5**, e983876. doi:10.4161/sgtp.29513

**Lappe-Siefke, C., Goebbels, S., Gravel, M., Nicksch, E., Lee, J., Braun, P. E., Griffiths, I. R. and Nave, K. A.** (2003). Disruption of Cnp1 uncouples oligodendroglial functions in axonal support and myelination. *Nat. Genet.* **33**, 366-374. doi:10.1038/ng1095

**Laursen, L. S., Chan, C. W. and Ffrench-Constant, C.** (2009). An integrin-contactin complex regulates CNS myelination by differential Fyn phosphorylation. *J. Neurosci.* **29**, 9174-9185. doi:10.1523/JNEUROSCI.5942-08.2009

**Legate, K. R., Montanez, E., Kudlacek, O. and Füssler, R.** (2006). ILK, PINCH and parvin: the tIPP of integrin signalling. *Nat. Rev. Mol. Cell Biol.* **7**, 20-31. doi:10.1038/nrm1789

**Legate, K. R., Wickström, S. A. and Fässler, R.** (2009). Genetic and cell biological analysis of integrin outside-in signaling. *Genes Dev.* **23**, 397-418. doi:10.1101/gad.1758709

**Li, F., Zhang, Y. and Wu, C.** (1999). Integrin-linked kinase is localized to cell-matrix focal adhesions but not cell-cell adhesion sites and the focal adhesion localization of integrin-linked kinase is regulated by the PINCH-binding ANK repeats. *J. Cell Sci.* **112**, 4589-4599. doi:10.1242/jcs.112.24.4589

**Li, S., Bordoy, R., Stanchi, F., Moser, M., Braun, A., Kudlacek, O., Wewer, U. M., Yurchenco, P. D. and Fässler, R.** (2005). PINCH1 regulates cell-matrix and cell-cell adhesions, cell polarity and cell survival during the peri-implantation stage. *J. Cell Sci.* **118**, 2913-2921. doi:10.1242/jcs.02422

**Liang, X., Draghi, N. A. and Resh, M. D.** (2004). Signaling from integrins to Fyn to Rho family GTPases regulates morphologic differentiation of oligodendrocytes. *J. Neurosci.* **24**, 7140-7149. doi:10.1523/JNEUROSCI.5319-03.2004

**Liu, H., Yang, Y., Xia, Y., Zhu, W., Leak, R. K., Wei, Z., Wang, J. and Hu, X.** (2017). Aging of cerebral white matter. *Ageing Res. Rev.* **34**, 64-76. doi:10.1016/j.arr.2016.11.006

**Lord, S. J., Velle, K. B., Mullins, R. D. and Fritz-Laylin, L. K.** (2020). SuperPlots: communicating reproducibility and variability in cell biology. *J. Cell Biol.* **219**, e202001064. doi:10.1083/jcb.202001064

**Manser, E., Leung, T., Salihuddin, H., Zhao, Z.-S. and Lim, L.** (1994). A brain serine/threonine protein kinase activated by Cdc42 and Rac1. *Nature* **367**, 40-46. doi:10.1038/367040a0

**Michalski, J.-P., Cummings, S. E., O'meara, R. W. and Kothary, R.** (2016). Integrin-linked kinase regulates oligodendrocyte cytoskeleton, growth cone, and adhesion dynamics. *J. Neurochem.* **136**, 536-549. doi:10.1111/jnc.13446

**Montanez, E., Wickström, S. A., Altstätter, J., Chu, H. and Fässler, R.** (2009). Alpha-parvin controls vascular mural cell recruitment to vessel wall by regulating RhoA/ROCK signalling. *EMBO J.* **28**, 3132-3144. doi:10.1038/emboj.2009.295

**Montanez, E., Karakose, E., Tischner, D., Villunger, A. and Fassler, R.** (2012). PINCH-1 promotes Bcl-2-dependent survival signalling and inhibits JNK-mediated apoptosis in the primitive endoderm. *J. Cell Sci.* **125**, 5233-5240. doi:10.1242/jcs.112029

**Montani, L., Buerki-Thurnherr, T., De Faria, J. P., Pereira, J. A., Dias, N. G., Fernandes, R., Goncalves, A. F., Braun, A., Benninger, Y., Böttcher, R. T. et al.** (2014). Profilin 1 is required for peripheral nervous system myelination. *Development* **141**, 1553-1561. doi:10.1242/dev.101840

**Nave, K.-A. and Werner, H. B.** (2014). Myelination of the nervous system: mechanisms and functions. *Annu. Rev. Cell Dev. Biol.* **30**, 503-533. doi:10.1146/annurev-cellbio-100913-013101

**Nawaz, S., Sánchez, P., Schmitt, S., Snaidero, N., Mitkovski, M., Velte, C., Brückner, B. R., Alexopoulos, I., Czopka, T., Jung, S. Y. et al.** (2015). Actin filament turnover drives leading edge growth during myelin sheath formation in the central nervous system. *Dev. Cell* **34**, 139-151. doi:10.1016/j.devcel.2015.05.013

**Nodari, A., Zambroni, D., Quattrini, A., Court, F. A., D'urso, A., Recchia, A., Tybulewicz, V. L., Wrabetz, L. and Feltri, M. L.** (2007). β1 integrin activates Rac1 in Schwann cells to generate radial lamellae during axonal sorting and myelination. *J. Cell Biol.* **177**, 1063-1075. doi:10.1083/jcb.200610014

**O'meara, R. W., Michalski, J. P., Anderson, C., Bhanot, K., Rippstein, P. and Kothary, R.** (2013). Integrin-linked kinase regulates process extension in oligodendrocytes via control of actin cytoskeletal dynamics. *J. Neurosci.* **33**, 9781-9793. doi:10.1523/JNEUROSCI.5582-12.2013

**Patzig, J., Erwig, M. S., Tenzer, S., Kusch, K., Dibaj, P., Mobius, W., Goebbels, S., Schaeren-Wiemers, N., Nave, K. A. and Werner, H. B.** (2016). Septin/anillin filaments scaffold central nervous system myelin to accelerate nerve conduction. *Elife* **5**, e17119. doi:10.7554/eLife.17119

**Pedraza, C. E., Taylor, C., Pereira, A., Seng, M., Tham, C. S., Izrael, M. and Webb, M.** (2014). Induction of oligodendrocyte differentiation and in vitro myelination by inhibition of rho-associated kinase. *ASN Neuro* **6**, 1759091414538134. doi:10.1177/1759091414538134

**Pereira, J. A., Benninger, Y., Baumann, R., Goncalves, A. F., Özçelik, M., Thurnherr, T., Tricaud, N., Meijer, D., Fässler, R., Suter, U. et al.** (2009). Integrin-linked kinase is required for radial sorting of axons and Schwann cell remyelination in the peripheral nervous system. *J. Cell Biol.* **185**, 147-161. doi:10.1083/jcb.200809008

**Peters, A.** (2002). The effects of normal aging on myelin and nerve fibers: a review. *J. Neurocytol.* **31**, 581-593. doi:10.1023/A:1025731309829
**Peters, A., Rosene, D. L., Moss, M. B., Kemper, T. L., Abraham, C. R., Tigges, J. and Albert, M. S.** (1996). Neurobiological bases of age-related cognitive decline in the rhesus monkey. *J. Neuropathol. Exp. Neurol.* **55**, 861-874. doi:10.1097/00005072-199608000-00001
**Qin, J. and Wu, C.** (2012). ILK: a pseudokinase in the center stage of cell-matrix adhesion and signaling. *Curr. Opin. Cell Biol.* **24**, 607-613. doi:10.1016/j.ceb.2012.06.003
**Raff, M. C., Durand, B. and Gao, F. B.** (1998). Cell number control and timing in animal development: the oligodendrocyte cell lineage. *Int. J. Dev. Biol.* **42**, 263-267.
**Rajasekharan, S., Bin, J. M., Antel, J. P. and Kennedy, T. E.** (2010). A central role for RhoA during oligodendroglial maturation in the switch from netrin-1-mediated chemorepulsion to process elaboration. *J. Neurochem.* **113**, 1589-1597. doi:10.1111/j.1471-4159.2010.06717.x
**Rearden, A.** (1994). A new LIM protein containing an autoepitope homologous to 'senescent cell antigen'. *Biochem. Biophys. Res. Commun.* **201**, 1124-1131. doi:10.1006/bbrc.1994.1822
**Sadian, Y., Gatsogiannis, C., Patasi, C., Hofnagel, O., Goody, R. S., Farkašovský, M. and Raunser, S.** (2013). The role of Cdc42 and Gic1 in the regulation of septin filament formation and dissociation. *Elife* **2**, e01085. doi:10.7554/eLife.01085
**Sander, E. E., Van Delft, S., ten Klooster, J. P., Reid, T., Van Der Kammen, R. A., Michiels, F. and Collard, J. G.** (1998). Matrix-dependent Tiam1/Rac signaling in epithelial cells promotes either cell-cell adhesion or cell migration and is regulated by phosphatidylinositol 3-kinase. *J. Cell Biol.* **143**, 1385-1398. doi:10.1083/jcb.143.5.1385
**Schindelin, J., Arganda-Carreras, I., Frise, E., Kaynig, V., Longair, M., Pietzsch, T., Preibisch, S., Rueden, C., Saalfeld, S., Schmid, B. et al.** (2012). Fiji: an open-source platform for biological-image analysis. *Nat. Methods* **9**, 676-682. doi:10.1038/nmeth.2019
**Seixas, A. I., Azevedo, M. M., Paes De Faria, J., Fernandes, D., Mendes Pinto, I. and Relvas, J. B.** (2019). Evolvability of the actin cytoskeleton in oligodendrocytes during central nervous system development and aging. *Cell. Mol. Life Sci.* **76**, 1-11. doi:10.1007/s00018-018-2915-8
**Sirajuddin, M., Farkasovsky, M., Hauer, F., Kühlmann, D., Macara, I. G., Weyand, M., Stark, H. and Wittinghofer, A.** (2007). Structural insight into filament formation by mammalian septins. *Nature* **449**, 311-315. doi:10.1038/nature06052
**Smeeton, J., Zhang, X., Bulus, N., Mernaugh, G., Lange, A., Karner, C. M., Carroll, T. J., Fässler, R., Pozzi, A., Rosenblum, N. D. et al.** (2010). Integrin-linked kinase regulates p38 MAPK-dependent cell cycle arrest in ureteric bud development. *Development* **137**, 3233-3243. doi:10.1242/dev.052845
**Snaidero, N. and Simons, M.** (2017). The logistics of myelin biogenesis in the central nervous system. *Glia* **65**, 1021-1031. doi:10.1002/glia.23116
**Snaidero, N., Möbius, W., Czopka, T., Hekking, L. H., Mathisen, C., Verkleij, D., Goebbels, S., Edgar, J., Merkler, D., Lyons, D. A. et al.** (2014). Myelin membrane wrapping of CNS axons by PI(3,4,5)P3-dependent polarized growth at the inner tongue. *Cell* **156**, 277-290. doi:10.1016/j.cell.2013.11.044
**Southwood, C., He, C., Garbern, J., Kamholz, J., Arroyo, E. and Gow, A.** (2004). CNS myelin paranodes require Nkx6-2 homeoprotein transcriptional activity for normal structure. *J. Neurosci.* **24**, 11215-11225. doi:10.1523/JNEUROSCI.3479-04.2004
**Stanchi, F., Bordoy, R., Kudlacek, O., Braun, A., Pfeifer, A., Moser, M. and Fässler, R.** (2005). Consequences of loss of PINCH2 expression in mice. *J. Cell Sci.* **118**, 5899-5910. doi:10.1242/jcs.02686
**Thurnherr, T., Benninger, Y., Wu, X., Chrostek, A., Krause, S. M., Nave, K.-A., Franklin, R. J., Brakebusch, C., Suter, U. and Relvas, J. B.** (2006). Cdc42 and Rac1 signaling are both required for and act synergistically in the correct formation of myelin sheaths in the CNS. *J. Neurosci.* **26**, 10110-10119. doi:10.1523/JNEUROSCI.2158-06.2006
**Tu, Y., Li, F., Goicoechea, S. and Wu, C.** (1999). The LIM-only protein PINCH directly interacts with integrin-linked kinase and is recruited to integrin-rich sites in spreading cells. *Mol. Cell. Biol.* **19**, 2425-2434. doi:10.1128/MCB.19.3.2425
**Vaynberg, J., Fukuda, T., Chen, K., Vinogradova, O., Velyvis, A., Tu, Y., Ng, L., Wu, C. and Qin, J.** (2005). Structure of an ultraweak protein-protein complex and its crucial role in regulation of cell morphology and motility. *Mol. Cell* **17**, 513-523. doi:10.1016/j.molcel.2004.12.031
**Vaynberg, J., Fukuda, K., Lu, F., Bialkowska, K., Chen, Y., Plow, E. F. and Qin, J.** (2018). Non-catalytic signaling by pseudokinase ILK for regulating cell adhesion. *Nat. Commun.* **9**, 4465. doi:10.1038/s41467-018-06906-7
**Velyvis, A., Vaynberg, J., Yang, Y., Vinogradova, O., Zhang, Y., Wu, C. and Qin, J.** (2003). Structural and functional insights into PINCH LIM4 domain-mediated integrin signaling. *Nat. Struct. Biol.* **10**, 558-564. doi:10.1038/nsb938
**Wang, H., Rusielewicz, T., Tewari, A., Leitman, E. M., Einheber, S. and Melendez-Vasquez, C. V.** (2012). Myosin II is a negative regulator of oligodendrocyte morphological differentiation. *J. Neurosci. Res.* **90**, 1547-1556. doi:10.1002/jnr.23036
**Wickström, S. A., Lange, A., Montanez, E. and Fässler, R.** (2010). The ILK/PINCH/parvin complex: the kinase is dead, long live the pseudokinase!. *EMBO J.* **29**, 281-291. doi:10.1038/emboj.2009.376
**Wiesner, S., Legate, K. R. and Fässler, R.** (2005). Integrin-actin interactions. *Cell. Mol. Life Sci.* **62**, 1081-1099. doi:10.1007/s00018-005-4522-8
**Wu, C.** (2004). The PINCH-ILK-parvin complexes: assembly, functions and regulation. *Biochim. Biophys. Acta* **1692**, 55-62. doi:10.1016/j.bbamcr.2004.01.006
**Wu, X., Quondamatteo, F., Lefever, T., Czuchra, A., Meyer, H., Chrostek, A., Paus, R., Langbein, L. and Brakebusch, C.** (2006). Cdc42 controls progenitor cell differentiation and β-catenin turnover in skin. *Genes Dev.* **20**, 571-585. doi:10.1101/gad.361406
**Ximerakis, M., Lipnick, S. L., Innes, B. T., Simmons, S. K., Adiconis, X., Dionne, D., Mayweather, B. A., Nguyen, L., Niziolek, Z., Ozek, C. et al.** (2019). Single-cell transcriptomic profiling of the aging mouse brain. *Nat. Neurosci.* **22**, 1696-1708. doi:10.1038/s41593-019-0491-3
**Xu, Z., Fukuda, T., Li, Y., Zha, X., Qin, J. and Wu, C.** (2005). Molecular dissection of PINCH-1 reveals a mechanism of coupling and uncoupling of cell shape modulation and survival. *J. Biol. Chem.* **280**, 27631-27637. doi:10.1074/jbc.M504189200
**Yang, H., Lin, L., Sun, K., Zhang, T., Chen, W., Li, L., Xie, Y., Wu, C., Wei, Z. and Yu, C.** (2021). Complex structures of Rsu1 and PINCH1 reveal a regulatory mechanism of the ILK/PINCH/Parvin complex for F-actin dynamics. *Elife* **10**. e64395. doi:10.7554/eLife.64395.sa2
**Zhang, Y., Chen, K., Guo, L. and Wu, C.** (2002a). Characterization of PINCH-2, a new focal adhesion protein that regulates the PINCH-1-ILK interaction, cell spreading, and migration. *J. Biol. Chem.* **277**, 38328-38338. doi:10.1074/jbc.M205576200
**Zhang, Y., Chen, K., Tu, Y., Velyvis, A., Yang, Y., Qin, J. and Wu, C.** (2002b). Assembly of the PINCH-ILK-CH-ILKBP complex precedes and is essential for localization of each component to cell-matrix adhesion sites. *J. Cell Sci.* **115**, 4777-4786. doi:10.1242/jcs.00166
**Zhang, Y., Chen, K., Sloan, S. A., Bennett, M. L., Scholze, A. R., O'keeffe, S., Phatnani, H. P., Guarnieri, P., Caneda, C., Ruderisch, N. et al.** (2014). An RNA-sequencing transcriptome and splicing database of glia, neurons, and vascular cells of the cerebral cortex. *J. Neurosci.* **34**, 11929-11947. doi:10.1523/JNEUROSCI.1860-14.2014
**Zuchero, J. B., Fu, M.-M., Sloan, S. A., Ibrahim, A., Olson, A., Zaremba, A., Dugas, J. C., Wienbar, S., Caprariello, A. V., Kantor, C. et al.** (2015). CNS myelin wrapping is driven by actin disassembly. *Dev. Cell* **34**, 152-167. doi:10.1016/j.devcel.2015.06.011